AD-A189 299 OPTICAL PROPERTIES OF COMPRESSIBLE INHOMOGENEOUS SHEAR LAYERS RELEVANT TO HIGH POWER LASERS(U) WASHINGTON UNIV SEATTLE W H CHRISTIANSEN 30 SEP 87 AFOSR-TR-87-1750 1/1

UNCLASSIFIED AFOSR-83-0059 F/G 9/3 NL

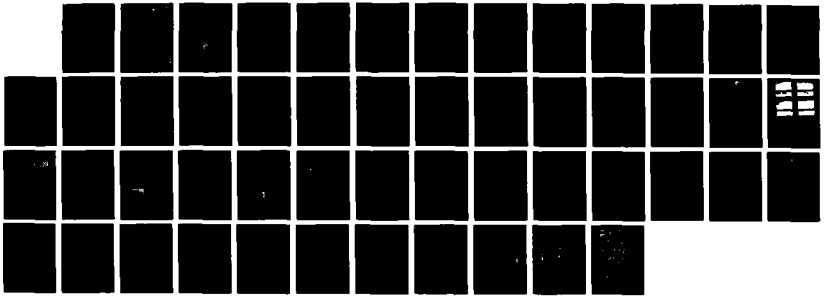

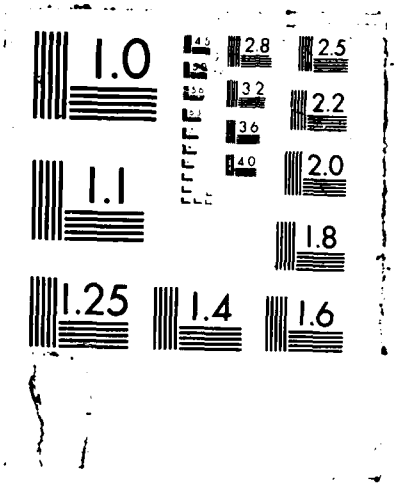
1.0
1.1
1.25
1.4
1.6
1.8
2.0
2.2
2.5
2.8
3.2
3.6
4.0

UNCLASSIFIE

SECURITY CLASSIFICATION OF TH

Rec'd 19 Oct 87
Acc 27 Nov 87

AD-A189 299

ON PAGE

TIC FILE COPY

1a. REPORT SECURITY CLASSIFICA UNCLASSIFIED	TIVE MARKINGS
2a. SECURITY CLASSIFICATION AUTHORITY	3. DISTRIBUTION / AVAILABILITY OF REPORT APPROVED FOR PUBLIC RELEASE DISTRIBUTION IS UNLIMITED
2b. DECLASSIFICATION / DOWNGRADING SCHEDULE	
4. PERFORMING ORGANIZATION REPORT NUMBER(S)	5. MONITORING ORGANIZATION REPORT NUMBER(S) AFOSR-TR- 87-1750
6a. NAME OF PERFORMING ORGANIZATION UNIVERSITY OF WASHINGTON 6b. OFFICE SYMBOL (If applicable)	7a. NAME OF MONITORING ORGANIZATION AFOSR/NA
6c. ADDRESS (City, State, and ZIP Code) UNIV OF WASH SEATLE WASHINGTON 98195	7b ADDRESS (City, State, and ZIP Code) BUILDING 410 BOLLING AFB, DC 20332-6448
8a. NAME OF FUNDING / SPONSORING ORGANIZATION AFOSR 8b. OFFICE SYMBOL (If applicable) NA	9. PROCUREMENT INSTRUMENT IDENTIFICATION NUMBER AFOSR-83-0059
8c. ADDRESS (City, State, and ZIP Code) BUILDING 410 BOLLING AFB, DC 20332-6448	10. SOURCE OF FUNDING NUMBERS PROGRAM ELEMENT NO. 61102F; PROJECT NO. 2307; TASK NO. A2; WORK UNIT ACCESSION NO.

11 TITLE (Include Security Classification)
(U)OPTICAL PROPERTIES OF COMPRESSIBLE INHOMOGENEOUS SHEAR LAYERS RELEVANT TO HIGH POWER LASERS

12. PERSONAL AUTHOR(S)
W. CHRISTIANSEN

13a. TYPE OF REPORT	13b. TIME COVERED	14. DATE OF REPORT (Year, Month, Day)	15 PAGE COUNT
FINAL TECH	FROM 2/1/83 TO 5/30/87	9/30/87	46

16. SUPPLEMENTARY NOTATION

17 COSATI CODES			18 SUBJECT TERMS (Continue on reverse if necessary and identify by block number)
FIELD	GROUP	SUB-GROUP	SHEAR LAYERS, LASER OPTICAL DEGREDATION, REFRACTIVE INDICES

19 ABSTRACT (Continue on reverse if necessary and identify by block number)

SHEAR LAYERS AND WAKES ARE A MAJOR SOURCE OF OPTICAL DEGREDATION IN FLOW LASERS. THE STRUCTURE OF THESE FLOWS HAS BEEN STUDIED EXPERIMENTALLY WITH SPECIAL ATTENTION GIVEN TO THEIR OPTICAL PROPERTIES. GASES WITH DIFFERENT REFRACTIVE INDICES WERE INVESTIGATED AND THE EFFECTS OF DENSITY RATIO AND MACH NUMBER WERE MEASURED. THE TIME AVERAGED OPTICAL PROPERTIES OF INHOMOGENIOUS SHEAR LAYERS IS REPORTED HERE WHERIN THE PRINCIPLE FAR FIELD MEASUREMENT WAS THE STREHL RATIO. MODIFICATION OF THE APPARATUS OF THE SHEAR IS DISCUSSED.

DTIC ELECTE JAN 07 1988 S D

20 DISTRIBUTION / AVAILABILITY OF ABSTRACT ☐ UNCLASSIFIED/UNLIMITED ☒ SAME AS RPT ☐ DTIC USERS	21 ABSTRACT SECURITY CLASSIFICATION UNCLASSIFIED
22a. NAME OF RESPONSIBLE INDIVIDUAL JAMES M. McMICHAEL	22b TELEPHONE (Include Area Code) 202-767-4935
	22c OFFICE SYMBOL AFOSR/NA

DD FORM 1473, 84 MAR 83 APR edition may be used until exhausted
All other editions are obsolete

SECURITY CLASSIFICATION OF THIS PAGE
UNCLASSIFIED

University of Washington

Final Technical Report 2/83 - 5/31/87
AFOSR Contract #83-0059
Walter H. Christiansen

OPTICAL PROPERTIES OF COMPRESSIBLE
INHOMOGENEOUS SHEAR LAYERS
RELEVANT TO HIGH POWER LASERS

Aerospace and Energetics Research Program

Final Technical Report 2/83 - 5/31/87
AFOSR Contract #83-0059
Walter H. Christiansen

OPTICAL PROPERTIES OF COMPRESSIBLE INHOMOGENEOUS SHEAR LAYERS RELEVANT TO HIGH POWER LASERS

Final Technical Report 2/83 - 5/31/87
AFOSR Contract #83-0059
Walter H. Christiansen

OPTICAL PROPERTIES OF COMPRESSIBLE INHOMOGENEOUS SHEAR LAYERS RELEVANT TO HIGH POWER LASERS

ABSTRACT

Shear layers and wakes are a major source of optical degradation in flow lasers. The structure of these flows has been studied experimentally with special attention given to their optical properties. Gases with different refractive indices were investigated and the effects of density ratio and Mach number were measured. The time averaged optical properties of inhomogeneous shear layers are reported here wherein the principle for field measurement was the Strehl ratio. Modification of the apparatus for low speed measurement, including periodic forcing of the shear is discussed.

I. INTRODUCTION

Fluid mechanics is involved in many lasing processes and the flow field must be of excellent optical quality so that a near diffraction limited laser beam may be attained. With the general trend of laser development towards shorter wavelenghts, the fluid optics challenge is increased considerably. In general, the conditioning of the gas laser cavity or external flow effects will continue to be a problem area. The fluid mechanical sources of fluid possible optical difficulties must be carefully examined and understood. It is known that phase distribution as well as, to a lesser degree, amplitude distribution across a coherent beam determines beam quality. We studied basic fluid mechanical properties of compressible shear layers and their effect on the phase distribution of a laser beam.

The 2-D inhomogeneous shear layer is chosen for a number of reasons. It is a simple and well studied flow, at least a low Mach number, M. However, there is no experimental optical data which concentrates on the coherent effects produced by the layer and the extent of the mixing interface on optics. Part of the research involves studying the properties of single two-dimensional shear layers at high Mach numbers and Reynolds numbers appropriate for high power lasers. Exprimentally this involves a systematic investigation with independent control of density ratio and compressibility effects of the free jets, which has not been done before. The optical quality of each shear layer was measured by examining the farfield diffraction pattern of laser beams passing through the layer. We hoped to understand and to predict compressible shear layer growth rate and optical performance on the basis of this study. Ways of controlling the optical degradation due to these layers has been suggested too. The 2-D layer is now being observed using controlled perturbation techniques which may be used to

advantage. The structures of these layers, when subjected to small but controlled perturbations, change leading to a rapid change in the mixing rate and probably the optical quality of the layer.

In the following section we will discuss our progress during this grant.

II. PROGRESS DURING GRANT PERIOD

a. Equipment and Setup

We were forced to move the experimental apparatus to a new location early in our program. The new laboratory (location in the AERB) resulted in improved apparatus and larger mass flow capability than from the previous setup. As part of the move, a new and larger capacity gas supply and metering system was constructed.

The test gases were ducted away from the optical table area after being discharged by the free jet, otherwise there would be optical interference with the diagnostic systems. The exhaust system carries the spent test gases away from the optical table and discharges them outside the laboratory building. The modest suction required is provided by an ejector in the exhaust ducting.

Substantial changes were made in the schlieren and interferometer optical diagnostic systems. Both systems were increased to 7.5 cm aperture (from earlier aperture of 4 cm) and the schlieren system was further modified to permit observation parallel and perpendicular to the shear layer simultaneously. The Mach-Zehnder interferometer system uses 6.5 cm beam splitters and mirrors and a new 7.5 cm beam-expanding telescope was built. The equipment includes a ruby laser and another Galilean beam expanding-telescope.

Nozzle exit dimensions chosen were 1.4 cm × 1.4 cm for Mach numbers up to 2.0. These represented a compromise between having a realistic nozzle dimension and the prohibitive expenses associated with large test gas mass flows. Reynolds numbers based on the nozzle exit dimensions will vary from 1.6×10^5 at M = 0.5 to 1.4×10^6 at M =2. A sketch of the test section is shown in Fig. 1 for the reader's convenience.

b. Observations and Tests

During the first part of this program subsonic shear layers were investigated. Shear layer growth rates for jet Mach numbers of 0.1, 0.3 and 0.6 were measured using a Mach-Zehnder interferometer. Interferograms using a He-Ne laser source were obtained for jets with various density ratios. Time-averaged optical density ($\beta_{\rho=n=-1}$) profiles through shear layers were calculated using such data. The results were compared with data available in the literature at low Mach numbers and fairly good agreement was achieved. We have observed a 30% growth rate reduction with the increase of Mach number from 0.1 to 0.6. Higher subsonic Mach number tests have been tried with Mach-Zehnder interferometers, but the optical quality of long exposure interferograms are poor due to loss of optical contrast. Stop action schlieren photographs were taken for various jets of gas at Mach numbers of 0.1, 0.6 and 0.9. The density ratio was varied from 0.66 to 7.2. For the lower Mach number jets coherent structure is not clear. Pictures were also taken simultaneously normal to the shear layer. Time averaged schlieren photographs have provided qualitative measurements of the shear layer growth rates. A reduction in the growth rate of shear layers with increasing Mach number and density ratio was observed.

Stop-action interferograms viewed normal to the turbulent interface have been taken for all the test gases. Such data provide near-field phase infromation. A package of software for automated data reduction using digital reading and processing of interferograms on an Apple II computer was developed. With the aid of this program, we were able to calculate the phase degradation of a ruby laser beam as a function of the distance from the exit of nozzle.

Papers were published related to the work on this project. The first deals with the fluid mechanical aspects of the program and was presented at the 17th AIAA Fluid Dynamics, Plasma Dyanmics and Lasers Conference in June, 1984 The second paper deals with the optical properties of the shear layers and was presented at the Chemical Gas Flow Lasers Conference in August, 1984. A third paper on computer reduction of the interferograms was published in the Review of Scientific Instruments.

Testing of a shearing interferometer as a supplement for the Mach-Zehnder interferometry was initiated then. The shearing interferometer produces an interference pattern between two rays displaced a finite distance apart by the splitter plate. The interference pattern produced by the flow field does not give optical density, but optical density difference between a preset distance across the flow-field. The test results proved useful, but additional development was not warranted.

Later shear layer growth rates for Mach numbers in excess of 0.9 were measured using a shearing interferometer using a He-Ne laser source. Pulsed schlieren pictures were also taken of these flows. A series of stop action Mach-Zehnder interferograms of shear layers at Mach numbers up to 1.4 were also taken and some interesting features were observed. But the most consistent results on spreading rates came from long exposure schlieren

measurements. In these measurements, the shear layers spreading rates were seen to decrease significantly with increasing M. A density ratio effect (spreading rates decreasing with increasing λ_ρ) was also seen. Large scale coherent structures of the type well known in low speed shear layers were very obvious at M=0.1, were progressively less apparent at M=0.6 and M=0.9 and were apparently absent at M=1.4. The results of shear layer thickness measurements are shown in Figs. 2 and 3.

Experiments were carried out to investigate the optical properties of fast shear layers by means of far field diffraction patterns of a circular laser beam resulting from its passage through the layer. The focal plane energy distribution of the laser beam is the far field pattern that was measured as part of this program. For these experiments, two different sized parallel HeNe laser beams, one 0.5 cm in diameter and the other 1.0 cm in diameter, were used to produce the far-field information. Each beam was passed through a rectangular gas jet with cross section of 1.4 cm on a side bounded on three sides by glass walls. After passing through the shear layer and jet, the beam exited through the glass wall and was demagnified by a telescope for convenience. The modified Airy pattern image was thus produced. The far field images were than compared to the tare data taken in an identical manner, except without the gas jet and shear layer.

Optical quality measurements taken normal to the high subsonic flow shear layer were carried out using a cw HeNe light source to obtain time averaged results. The measurements concentrated on Strehl ratio and tilt aberration error. These results were obtained by using a new electronic digital image acquisition system. These measurements covering various Mach numbers, M, and density ratios, were published in two masters theses at the University by D. Higgins and T. Blum.

These results coupled with our previous shear layer measurements provided us with values of shear layer width to correlate with density ratio and Mach number. The near-field beam degradation may be related to the far-field intensity if the Strehl ratios are measured. Parameters such as the laser wave number, k, and the index refraction change, Δn, across the layer are known. The mean shear layer thickness, δ, is known from our fluid mechanical experiments. In the cases where no coherent structure is seen, the scale lengths may be assumed to be roughly proportional to the measured shear layer thickness. Under these conditions we may write the Strehl ratio as

$$\text{Strehl Ratio} = \exp\left(-\overline{\Delta\phi}^2\right) = \exp\left(-Ak^2\Delta n^2\delta^2\right)$$

Values of A were found for the range of interest based on our measurements of δ and Strehl ratio. This correlation relates the far-field performance to fluid mechanical parameters that are defined with respect to the mean thickness of the shear layer. A synopsis of this optical work has been published in the Proceedings of the International Conference on Fluid Mechanics in China 1987.

c. Low Speed Experimental Setup

The optical results in which large scale structures seem to assert an influence require additional testing. Because of experimental difficulties on the size of the apparatus and practical interest in low speed flow, the emphasis has been shifted from a high speed shear layer to the optics of low speed shear layers. This required a transition to a new flow facility which has been built. This new and much larger wind tunnel allows for larger test beams (diameter > 5.0 cm). In contrast to what was done earlier, two coplanar flows with velocities U_1 and U_2 and densities ρ_1 and ρ_2 initially

mix on contact at $x = 0$. Previously, only one free jet had been used. Now the velocity ratio can be varied. The Mach numbers of the flows are considerably less than one and should have no effect on the shear layer. In addition, each nozzle exit geometry has an aspect ratio of 4:1 in order to provide for better 2D flow characteristics and are enlarged considerably for ease of use. The overall flow consists of free-shear layer mixing between two parallel streams in the presence of walls which bound the streams.

This low speed test facility essentially consists of two independent side-by-side tunnels discharging into a common test section as shown in Fig. 4. Each channel was installed with one honeycomb and three screens to reduce the turbulence level of the freestream. A perforated plate was inserted in one of the channels to produce a velocity difference between the two streams. The nozzles have exit cross sections of 4" × 1" each. The turbulence level was measured by hot wires to be about 0.5% at the exit plane of the nozzles. A plexiglass test section was fabricated to be 12" long, 4" wide and 2" high. The top and bottom walls were adjustable so that the pressure gradient in the flow direction can be minimized. Under there conditions, the flow field is, on the basis of hot wire and optical measurements, very similar to those of others. Extensive depth hot wire measurements in perturbed flow are in the process of being obtained.

Using optically dissimilar gases provides differences in the index of refraction that can be used to study the flow and obtain optical details on the mixing process. A rectangular plenum chamber equipped with six small fans was utilized to supply air flow. Other gases were introduced from pressurized gas bottles for the dissimilar gas mixing layer case with an additional splitter plate. A thin oscillating flap with a width of 10 mm was added at the end of the splitter plate as a source of external

perturbation. It was suspended by a music wire under tension such that the flap could be oscillated around its leading edge by two voice coils at frequencies up to 200 cps and up to an amplitude of 2 mm (see Fig. 4). The second part of the preliminary investigation is the inhomogeneous mixing layer. Air-He and air-CO_2 mixing layers were chosen, because substantial index-refraction differences exist between these gases which are very good for schlieren and shadowgraph pictures. The experiment conditions were kept basically the same as the air to air mixing layer in order to be comparable. The instantaneous schlieren and shadowgraph pictures with both plan and side view in both inhomogeneous and homogeneous mixing layers have been done. With perturbation, the nature of large coherent structures in the spanwise direction is evident and showed in side and plan view pictures.

Our preliminary experimental results confirmed the two-dimensional nature of large streamwise coherent structures in both the homogeneous and inhomogeneous mixing layers. They are essentially a kind of instability wave having a natural frequency and are highly susceptible to external perturbation. This feature may make it possible to improve and finally control the optical properties of the mixing layer.

d) Numerical Modeling

While the project is largely experimental, numerical simulations of plane 2D mixing layers have also been initiated this year. Direct numerical simulations are currently being carried out by solving the nonsteady 2D Euler equations without employing sub-grid scale modeling.

Basically, we are applying MacCormack's finite volume methods to solve the Euler equations. Only the explicit scheme has been used at this time. Even for two dimensional flow, such a program is formidable and takes considerable computer time. Our initial results, for an air-air shear layer

with a velocity ratio of 1/2 show a normalized spreading rate of about 0.055. This is smaller, but consistent with some experimental observations which are about 0.06. Mean values of streamwise velocity show a characteristic spreading behavior. It seems that the mean growth of the shear layer is given quite well even if viscosity is not employed in the basic equations. However, considerable improvements in the code are needed for inhomogeneous flows. We are now computing two air streams with different enthalpies so that the density ratio is 1.1.

LIST OF PUBLICATIONS

Several recent publications have been wholly or partly supported by this AFOSR Grant. These publications are:

1. Bogdanoff, D.W., "The Optical Quality of Shear Layers: Prediction and Improvement Thereof," AIAA Journal 22, 58 (1984).

*2. Johari, H., Poling, H., Bogdanoff, D.W. and Christiansen, W.H., "A Preliminary Study of Optical Properties of Inhomogeneous Shear Layers," AIAA Preprint, 84-1622, 17th Fluid Dynamics, Plamsa Dynamics and Laser Conference, Snowmass, CO. 1984.

*3. Christiansen, W.H., Johari, H. and Bogdanoff, D.W., "A Study of Inhomogeneous Shear Layers and their Effect on Laser Beam Degradation," in the proceedings of the 5th Gas Flow and Chemical Laser Symposium, Oxford, England, pp. 349-350, 1984.

4. Bogdanoff, D.W., "Interferometric Measurement of Heterogeneous Shear Layer Spreading Rates,", AIAA Journal 22, 1550 (1984).

5. Poling, H.W., "Optical Properties of Shear Layers," MS in Aeronautics and Astronatics Thesis, University of Washington, 1985.

6. Chen, H-T. and Christiansen, W.H., "Simulated Method for the Determination of Density Profiles from Mach-Zehnder Interferograms," Rev. Sci. Instr., 56, 1619 (1985).

7. Higgins, D.R., "Laser Beam Degradation By an Innomogeneous Free Jet Mixing Layer," MS in Aeronautics and Astronautics, 1986.

8. Blum, T.C., "Far Field Optical Properties of Compressible Inhomogeneous Shear Layers," MS in Aeronautics and Astronautics, 1986.

*9. Christiansen, W.H., et al. "Optics of Inhomogeneous Shear Layers," Proceedings of the International Conference on Fluid Mechanics," Beijing, China, July (1987).

*10. Blum, T.C., "Far Field Optical Properties in Compressible Shear Layers," AIAA Preprint, 87-0147, 25th Aerospace Sciences Meeting, Reno, NV. 1987.

* Attached to this report.

PRESENTATIONS

1. Johari, H., et al. "A Preliminary Study of Optical Properties of Inhomogeneous Shear Layaers," 17th Fluid Dynamics, Plasma Dynamics and Laser Conference, 1984.
2. Christiansen, W.H., et al. "A Study of Inhomogeneous Shear Layers and Their Effect on Laser Beam Degradations," 5th Gas Flow and Chemical Laser Symposium, 1984.
3. Blum, T.C., "Far Field Optical Properties in Compressible Inhomogeneous Shear Layers," AIAA Region VI Student Conference, 1986.
4. Blum, T.C., "Far Field Optical Properties in Compressible Inhomogeneous Shear Layers," 25tn Aerospace Sciences Meeting, 1987.
5. Christiansen, W.H., et al. "Optics of Inhomogeneous Shear Layers," International Conference on Fluid Mechanics, Beijing, China, 1987.

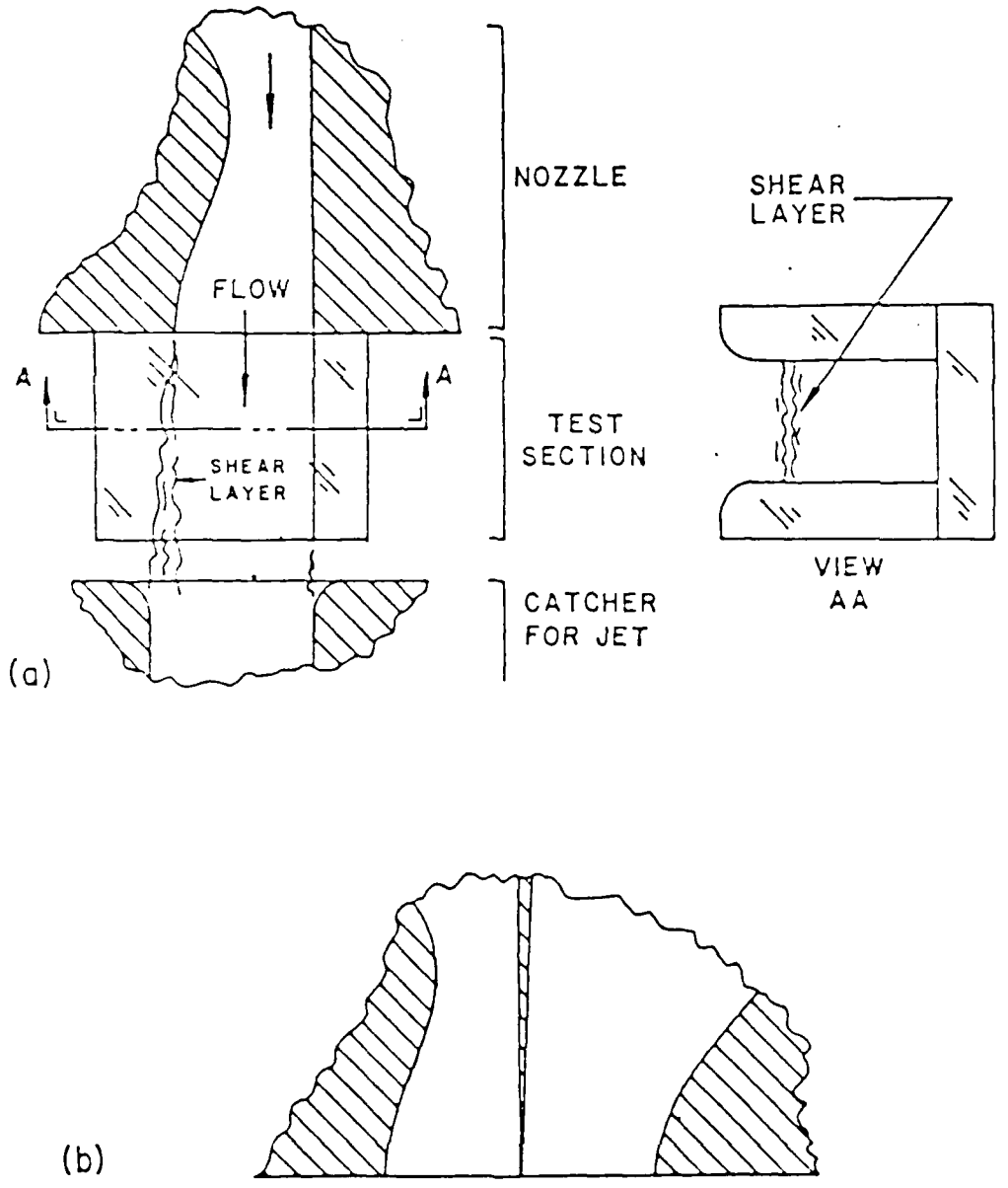

Fig. 1. Test section and typical nozzle for proposed research. (a) Configuration with single nozzle for initial contract period ($\dot{\omega}_u$=0). (b) Double nozzle configuration which may be used for later work ($\dot{\omega}_u \neq 0$).

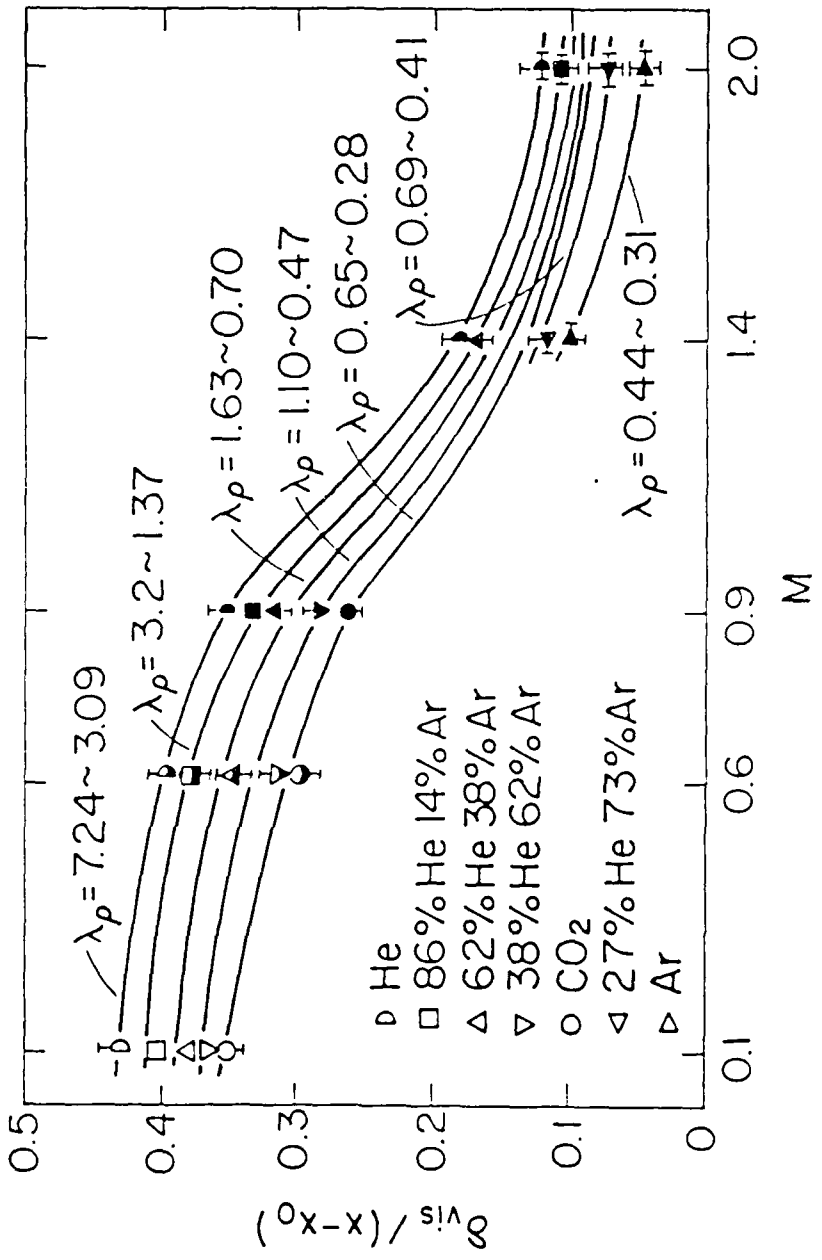

Fig. 2. Shear layer thickness vs Mach Number

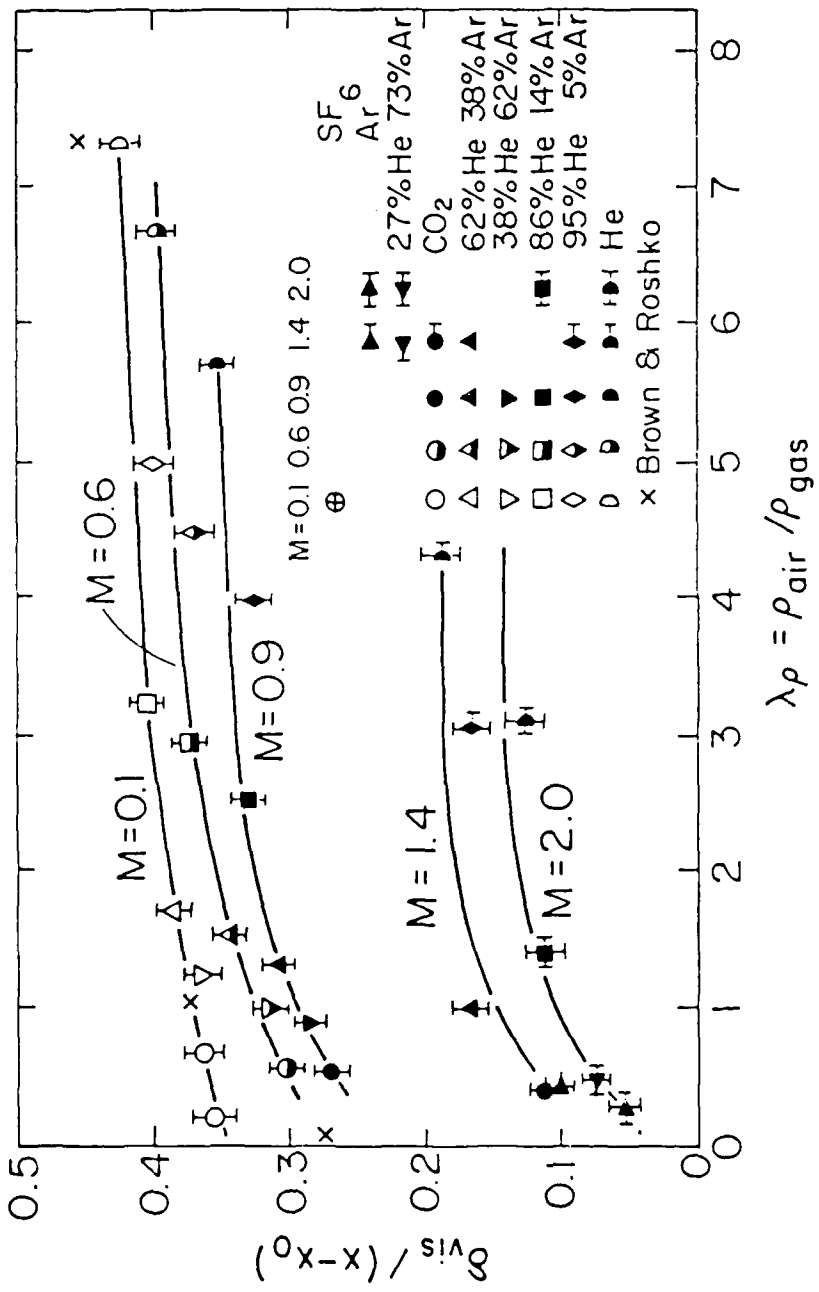

Fig. 3. Shear layer thickenss vs Density Ratio

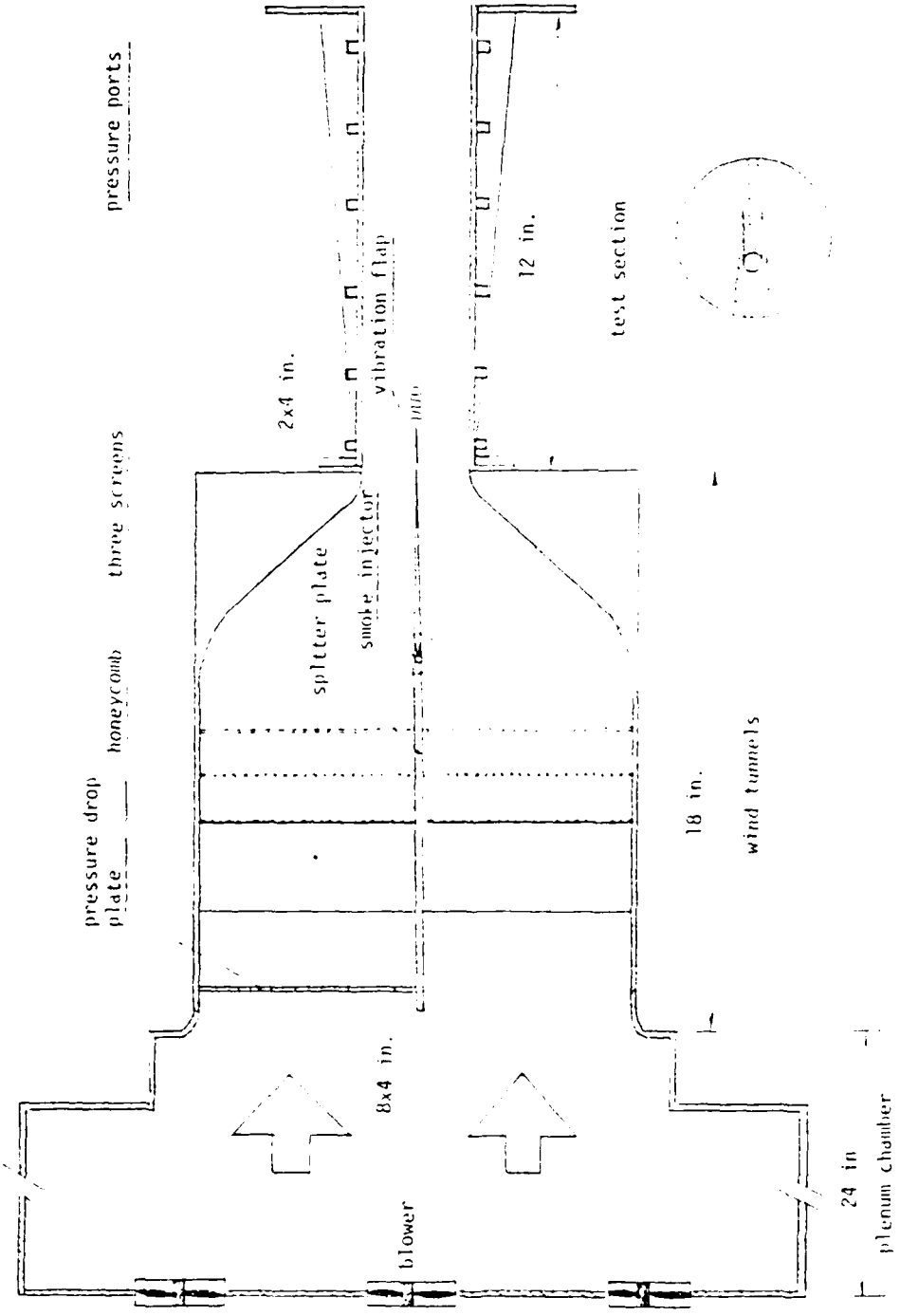

Fig. 4. Schematic diagram of apparatus.

A PRELIMINARY STUDY OF OPTICAL PROPERTIES OF INHOMOGENEOUS SHEAR LAYERS

Hamid Johari,* Hugh Poling,* H.T. Chen,** D.W. Bogdanoff+
and Walter H. Christiansen*
Department of Aeronautics and Astronautics
University of Washington
Seattle, Washington 98195

Abstract

Fluid mechanical and optical properties of two-dimensional, subsonic shear layers with zero velocity ratio have been investigated. Experimental measurements of shear layer growth rates and laser beam degradation for propagation normal to the turbulent interface are presented. From schlieren photographs and long exposure interferograms taken parallel to the shear layer, growth rates were found to decrease with increasing Mach number. Coherent structure was observed at jet Mach numbers of 0.1, while the shear layer structure appears to be more random at jet Mach numbers of 0.6 to 0.9. Interferograms taken normal to the shear layer show that the greatest beam degradation is for a helium jet since the net index of refraction difference across the shear layer is the largest. The helium jet also produced larger shear layer growth rate than the others. The least beam degradation was observed for a jet of a helium and argon mixture with a small refractive index change across the shear layer.

1. Introduction

There are numerous instances where laser beams encounter turbulent interfaces in high power gas laser technology. Shear layers and wakes occur in the resonators of most high power laser systems, but particularly in the gasdynamic laser and supersonic diffusion laser. The extraction of power usually involves passing the beam through interfaces which often involve dissimilar gases of different optical properties. Shear layers are also an important feature of aerodynamic windows (i.e., gas windows which separate the lasing medium from the surrounding environment by means of aerodynamic forces even with substantial pressure differences across the window). While a number of investigations[1,2,3] of the optical properties of this flow have been carried out, additional study is warranted to cover a wider range of experimental conditions.

A review of the literature on shear layers indicates that most experiments are restricted to low Mach numbers or, when compressibility is important, to conditions limited to those obtained from air streams of equal stagnation temperature rather than dissimilar gases. In the latter cases, Mach number and density ratio were varied simultaneously, making it difficult to separate the effects of compressibility and density ratio. The experimental conditions of the earlier work are shown in Fig. 1 by points in the λ_ρ and M_1 plane where λ_ρ is the density ratio and M_1 is the Mach number of the high speed gas stream. All the points are either incompressible results or fall along a single curved line. Representative values for high power laser resonators lie in the hatched areas in the λ_ρ-M_1 plane. The hatched area along $\lambda_\rho = 1$ in Fig. 1 is representative of refractive index matched aerodynamic windows.

The fluid dynamics and gas optical properties of single two-dimensional shear layers at Mach numbers and Reynolds numbers appropriate for high power lasers are being studied. Experimentally this involves a systematic investigation through independent control of density ratio and compressibility effects of the free jets. This is usually accomplished by using jets of various helium and argon mixtures. Of importance is the examination of compressible shear layers accompanying these jets for evidence of coherent, large scale vortical structures, since such large scale structures are even more troublesome optically than a random turbulent field.

This paper describes the construction and assembly of a subsonic nozzle system. The density fields showing shear layer spreading was measured using long-exposure interferograms. In addition, stop-action schlieren photographs have been taken with pictures taken simultaneously parallel and perpendicular to the shear layer These tests have been done at Mach numbers of 0.1, 0.6 and 0.9 with various density ratios. At the same test conditions, long exposure interferograms parallel to the shear layer using an He-Ne laser have been taken. This permits determination of the shear layer spreading rates. These growth rates are compared with the literature, thus checking the quality of the flow field and evaluating the interferometric technique. A particular aspect of this experiment is to study the effect of Mach number on large scale structures. Interferograms using a ruby laser beam perpendicular to the shear layer have been taken also. The photographs provide preliminary phase error data which are used to determine the scale size and amplitude of the refractive index perturbations in the shear layer and show the regions of the shear layer producing the most serious degradation of the laser beam. These measurements should enable one to identify the basic fluid mechanical optical effects of shear layers and their effect on far-field performance of a laser beam.

2. Flow Geometry and Measurement Techniques

A two-dimensional symmetric nozzle with a 1.4 cm square exit was employed to produce a subsonic shear layer. This investigation is focused on zero velocity ratio shear layers. A schematic view of the flow geometry is shown in Fig. 2. The nozzle is cut into a block of brass; another piece of brass forms the (side) cover. Turbulence is reduced by two orifice plates with 1.08 mm holes on a 1.75 mm square grid pattern. The nozzle has a 6:1 area contraction with straight (45°) sidewalls to

*Graduate Research Assistant, Dept. of Aeronautics & Astronautics; Student Member, AIAA.
**Visiting Research Associate, UW; Associate Professor, Institute of Mechanics, Chinese Academy of Sciences, Beijing, PRC.
+Research Engineer, Aerospace & Energetics Research Program; Member of AIAA.
‡Professor, Dept. of Aeronautics & Astronautics; Member, AIAA.

minimize boundary layer growth. The momentum thickness, θ, at the exit of nozzle was calculated to be 0.0027 cm for $M_1 = 0.1$. The nozzle plenum pressure is measured using a strain gauge pressure transducer connected to a pressure tap located 6 mm downstream of the second orifice plate.

The test section is formed from three flat plates of optical glass set up to be a continuation of the three walls of the nozzle. The open fourth side allows the room air to mix with the nozzle exit flow. The test section is 7.5 cm long. Jets of various helium and argon mixtures permit variations of density ratio at different flow conditions. The Reynolds number, based on the nozzle exit dimension, ranges from $3.1(10^4)$ to $3.3(10^5)$ for a mixture with $\lambda_\rho = 1$ and $M_1 = 0.1$ to 0.9, respectively. A catcher with a slight applied suction is placed at the end of the test section to remove the exhaust gases. The catcher entry has large radius edges and the width of the catcher opening is adjustable to accommodate various shear layer spreading rates.

Gas mixtures are supplied to the nozzle from a bank of gas cylinders. The arrangement allows four different mixtures to be tested with a particular optical diagnostic system. The system provides fine control of the nozzle mass flow rate over a nozzle exit Mach number range of 0.0-0.9. A quarter turn valve is used to start and stop the test runs. The valve is opened 2-3 secs for a test run. The highest mass flow rate used to date was 87 gm/sec at $M = 0.9$, $\lambda_\rho = 1$. The gases that have been tested are He, N_2, CO_2 and two mixtures consisting of 86 He/14 Ar and 38 He/62 Ar by volume.

The schlieren apparatus (Fig. 3) can be used to take simultaneous photographs parallel and normal to the shear layer. The light source is a 0.12 cm wide spark gap operated in dry nitrogen. The light duration is approximately 300 nsec. Two 7.6 cm diameter parabolic mirrors are used to produce parallel beams of light. The beams can be accurately aligned parallel and normal to the shear layer. After passing through the shear layer, the beams are focused on the knife edges by two additional mirrors. The shear layer is imaged on the two film planes at approximately unity magnification.

Long exposure interferograms were taken parallel to the shear layer with a Mach-Zehnder interferometer.[4] The system also uses 7.6 cm diameter optics. The optics are mounted in steel optical mounts which are in turn bolted to a 5 cm thick aluminum plate. This massive structure is useful to reduce the blurring of the long exposure interferogram due to acoustic radiation from the shear layer.

Two different laser light sources are used with the Mach-Zehnder interferometer. Long exposure photographs are taken using a 1 mW He-Ne laser as the light source. The He-Ne beam is expanded to a diameter of the optics using a telescope equipped with a spatial filter. An exposure time of 0.1 sec was generally used.

Optical quality data were obtained using short exposure interferograms taken normal to the shear layer. An actively Q-switched ruby laser was used as the light source. The pulse energy is about 20 mJ and the pulse length is 100 nsec. To obtain the necessary coherence length for interferometry, it is necessary to use an etalon as the laser output coupler. The beam is expanded using a simple uncoated negative lens. The beam is not parallel, but very slightly diverging while passing through the shear layer. This should produce only negligible distortion in the interferograms. The long exposure interferograms presented here were taken parallel to the shear layer; the short exposure interferograms were taken normal to the shear layer.

3. Shear Layer Spreading Measurements

Long exposure interferograms were used to measure the shear layer spreading rate. An exposure time of about 0.1 sec was used to give proper time-averaging. The mean growth rate of the index of refraction profiles of the shear layer were measured by counting the fringe shifts. If the mean fringe shift is denoted by ΔN, then

$$\Delta N = \frac{L}{\lambda}\Delta n = \frac{L}{\lambda}\Delta(\beta\rho) \quad , \quad n-1 = \beta\rho \quad ,$$

where L = optical path length,
λ = wavelength of the laser (6328Å),
ρ = density, and
β = Gladstone-Dale constant.

The change in $(\beta\rho)$ across the shear layer was calculated by measuring ΔN at four positions downstream of the nozzle exit.

Figure 4 is an interferogram for a gas mixture (38 He/62 Ar) having a density equal to that of air at room temperature at $M_1 = 0.3$. The flow is from left to right. The noble gas mixture is on the lower portion of the photograph while ambient air is at the top. Note that the pattern loses its contrast far from the nozzle exit. Other interferograms were taken at Mach numbers of 0.1, 0.3, and 0.6 for this mixture. A mixture of substantially different density ratio produced too many fringe shifts to be accurately analyzed by this technique. This set of data was read by hand which limits the resolution to about 0.2 fringe. Self-similar profiles were obtained using a computer program minimizing the mean square error of this profile.

The virtual origin, x_0, of the shear layer was calculated using this program to give the best fit linear growth rate. The root-mean-square error of the self-similarity profiles were about 5%. Figure 5 shows refractive index profiles plotted in non-dimensional coordinates for the interferogram shown in Fig. 4. The transverse coordinate is η and is defined as

$$\eta = y/(x-x_0) \quad .$$

The vertical axis of Fig. 5, labeled Index/Composition, refers to refractive index variation Δn inside the shear layer when non-dimensionalized by the difference of the index between the free stream and ambient air. The downstream position of each data set is also shown in the figure.

Figure 6 shows the best fit curve for three mean index profiles and Fiedler's[5] mean temperature data. The right hand portion of the graph shows the comparison between Fiedler's curve and the $M_1 = 0.1$ profile. The two curves agree reasonably well. The left hand side of Fig. 6 presents a comparison among $M_1 = 0.1$, 0.3, and 0.6 profiles. The general shape of the $M_1 = 0.3$ curve does not agree with the $M_1 = 0.1$, and 0.6 profiles. It shows a larger

growth rate than the two other cases. The reason is not known at this time. Also, note that the $M_1 = 0.6$ profile has a higher slope throughout the layer and gives a smaller growth rate than $M_1 = 0.1$. The data from Ref. 5 was chosen because the experiments are similar and the index profile data corresponds with temperature if one assumes Δn is proportional to density. Although the Mach numbers are different (in Fielder's case $M_1 = 0.02$), the Reynolds numbers are close, thus providing a good check on the results for the $M_1 = 0.1$ profile. For low speed flow, Mach number should not have any effect on the growth rate of the shear layer. A comparison among this data and that of Ref. 5 is presented in Table 1. For this data λ_ρ is nearly one. The Reynolds number of the flow is based on free stream properties and the maximum observed length of the shear layer, x_{max}. According to Bradshaw,[6] a free shear layer becomes self-similar with respect to Reynolds stresses at distances greater than 1000 momentum thicknesses (calculated at the nozzle exit). The ratio x_{max}/θ for this experiment is estimated to be clearly in excess of this requirement. The nondimensional shear layer thickness is δn which was defined by the slope of a straight line passing through the non-dimensional points $\Delta n = 0.2$ and $\Delta n = 0.8$. Lastly, $r_{0.5}$ represents the location of $\Delta n = 0.5$.

It is apparent from Fig. 6 and Table 1 that the lowest Mach number profile matches well with data from Ref. 5. The usual 5% and 95% points used in velocity profiles were not used for two reasons. First, refractive index profiles do not correspond necessarily to velocity profiles. Secondly, because of the large scatter in data around the asymptotic levels, it is much more accurate to use the 80% and 20% points. Most of the scatter in data is believed to be a result of manually reading the interferogram and possible changes in the tare interferogram. An automated system using computer graphics and a digital readout is being developed (see Appendix). The shear layer thickness is reduced by about 30% with an increase of M_1 from 0.12 to 0.58 whereas λ_ρ decreased only 10%. One might argue that this could be a *Re number effect since* it is tripled going from $M_1 = 0.1$ to $M_1 = 0.6$. However, Breidenthal,[7] has suggested that it cannot be purely a result of the change in the Reynolds number. Higher Reynolds number only affects the position of the virtual origin, x_o, and therefore the initial roll-up of the vortices. Another possible explanation is that acoustic radiation may interact with the pairing process of the vortices. Crow and Champagne[8] were able to change the growth rate of a jet radically by using external acoustic radiation through a loudspeaker at the frequency, $0.3\ U_1/D$. In this experiment the acoustic source was the jet itself rather than an external source. It is not clear if the effect would be the same, but acoustic noise may change the shear layer growth rate. Other possible effects exist. For example, dissipation heating of the middle region of the shear layer may be a factor. This latter effect would be more apparent at higher Mach numbers. More data is required to determine the cause of the growth rate reduction. Higher subsonic Mach number tests (mainly, $M_1 = 0.9$) have been tried. At present, the quality of the interferograms is poor due to loss of optical contrast. Various improvements are being instituted to improve the results at high Mach numbers.

4. Schlieren Observation of the Shear Layer

Schlieren photographs were taken for jets of CO_2, N_2, 38 He/62 Ar, 86 He/14 Ar and He at Mach numbers of 0.1, 0.6 and 0.9. Figures 7, (a) and (b) show photographs for the 86 He/14 Ar mixture at $M_1 = 0.1$. Figures 7, (c) and (d) show photographs at $M_1 = 0.6$ for the same mixture. Figures 7, (e) and (f) show photographs for CO_2 at $M_1 = 0.1$ and Figs. 7, (g) and (h), show photographs for CO_2 at $M_1 = 0.6$. The flow is from left to right in all the pictures in Fig. 7. In photographs viewing the growth rate, the jet is on the bottom while ambient air is at the top. The density ratio for the mixture is 3.2 for the low Mach number and 2.9 for the high speed case. The corresponding density ratios for CO_2 are 0.66 and 0.60.

The schlieren effect was quite small for N_2 and 38 He/62 Ar jets since the index of refraction difference was very slight at low Mach numbers. For most cases, shear layer growth rate estimated from the photographs decreased with increasing Mach number. An ensemble of just a few pictures gave results very close to that of mean interferometeric data for growth rate of the shear layer. At the lowest Mach number coherent structure[3] was observed in all cases. In the region close to the nozzle exit in Fig. 7(a), roll-up of the vortices is visible, while turbulence becomes evident in the regions further downstream. Figure 7(e) shows an unusually large roll-up of the vortices throughout the test section. At higher Mach number the coherent structure disappears and the flow seems to be more of a random nature (see Figs. 7(c) and 7(g)). In some cases the initial roll-up of vortices was observed even at $M_1 = 0.6$. Pictures taken normal to the shear layer at low Mach number show the spanwise-sinuous wiggles observed elsewhere[10] (see Figs. 7(b) and (f)). Upstream of the wiggles the flow is nearly two-dimensional, while downstream, small scale three-dimensional motions and streamwise streaks exist. It is believed that this is a manifestation of an initial three-dimensional instability and plays an important role in the introduction of small scale structure into the flow. At higher Mach number some structures and streamwise streaks are observable; however, they cannot be readily related to the wiggles in low Mach number flow (see Figs. 7(d) and (h)).

5. Optical Quality Measurements Normal to the Shear Layer

The main objective in this project is to determine the degradation of an optical beam due to refractive index fluctuation resulting from turbulence in a shear layer. Stop-action interferograms were taken normal to the shear layer, for various density ratios, to obtain near-field phase error data. Figure 8 shows three interferograms taken at $M_1 = 0.6$ and a tare (no-flow) interferogram. The density ratios are 0.60, 0.99, and 6.5 for CO_2, 38 He/62 Ar, and He, respectively. There is a striking difference between the index fluctuations, as expected.[1,2] The index of refraction difference between the jet and air at room temperature was lowest for the mixture ($\Delta n = 7.7 \times 10^{-5}$) and highest for He ($\Delta n = 2.35 \times 10^{-4}$). Qualitative estimates of the mean square phase error shows that the beam degradation is worse for CO_2 compared with the mixture by nearly one order of magnitude in the self-similar region. A He jet on the other hand

produces the most error, giving an order of magnitude increase in the mean square of the phase error over CO_2. These phase errors can be correlated to $(\Delta n)^2$ across the shear layer. Not only is Δn larger across the layer in the case of He jet, but the jet exhibits the largest growth rate among the gases being tested at this Mach number. At this time we are in the process of evaluating these data more completely using an automated data reduction system.

Acknowledgment

This research was sponsored by the Air Force Office of Scientific Research.

References

1. Legner, H.H., Otis, J.H., Theophanis, G.A., and Feinberg, R.M., "Laser Beam Degradation through Turbulent Interfaces," AIAA Paper 78-71, 1978.
2. Vu, B.T., Sutton, G.W., Theophanis, G.A., and Limpaecher, R., "Laser Beam Degradation through Optically Turbulent Mixing Layers," AIAA Paper 80.1414, 1980.
3. Bogdanoff, D.W. and Insuik, R.J., "Optical Quality of Supersonic Jets of Various Gases," Applied Optics, Vol. 21, No. 5, March 1982, pp. 893-903.
4. Liepmann, H.W. and Roshko, A., Elements of Gas Dynamics, Wiley, New York, 1952.
5. Fiedler, H.E., "Transport of Heat Across a Plane Turbulent Mixing Layer," Advances in Geophysics, Vol. 18A, Academic Press, New York, 1974, pp. 93-109.
6. Bradshaw, P., "The Effect of Initial Conditions on the Development of a Free Shear Layer," Journal of Fluid Mechanics, Vol. 26, Part 2, 1966, pp. 225-236.
7. Breidenthal, R.E., private communication, University of Washington.
8. Crow, S.L. and Champagne, F.H., "Orderly Structure in Jet Turbulence," Journal of Fluid Mechanics, Vol. 48, 1971, pp. 547-591.
9. Brown, G.L. and Roshko, A., "On Density Effects and Large Structure in Turbulent Mixing Layers," Journal of Fluid Mechanics, Vol. 64, Part 4, 1974, pp. 775-816.
10. Konrad, J.H., "An Experimental Investigation of Mixing in Two-Dimensional Turbulent Shear Flows with Applications to Diffusion-Limited Chemical Reactions," Project SQUID Technical Report CIT-8-PU, 1976.

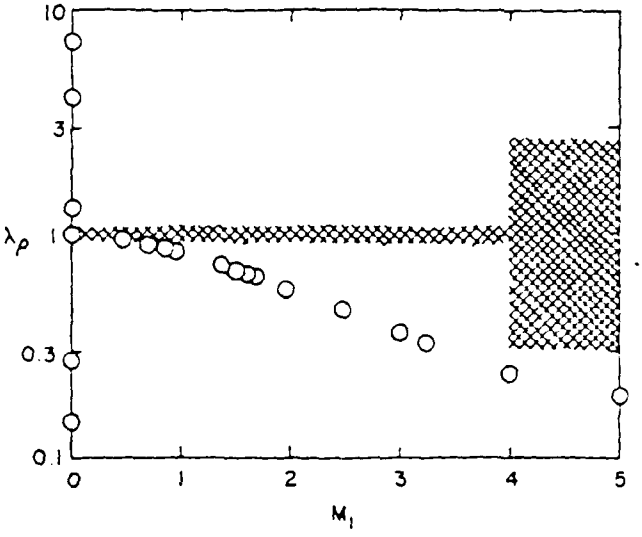

Fig. 1. λ_ρ vs. M_1 for previous work on two dimensional shear layers (circles). Hatched areas represent some shear layer conditions of interest in high power laser systems.

Author	M_1	λ_ρ	$Re_{x,max}$	$\frac{x_{max}}{\theta}$	Δn	$\eta_{0.5}$	$\frac{x_0}{x_{max}}$
Fiedler[5]	0.02	1.09	4.0×10^5	1400	0.26	-0.038	-0.071
This Work	0.12	1.10	8.4×10^4	1400	0.28	-0.046	-0.14
"	0.32	1.07	2.6×10^5	2600	0.20	-0.037	-0.21
"	0.58	0.99	2.8×10^5	1900	0.20	-0.047	-0.31

Table 1. Comparison of mean index profiles.

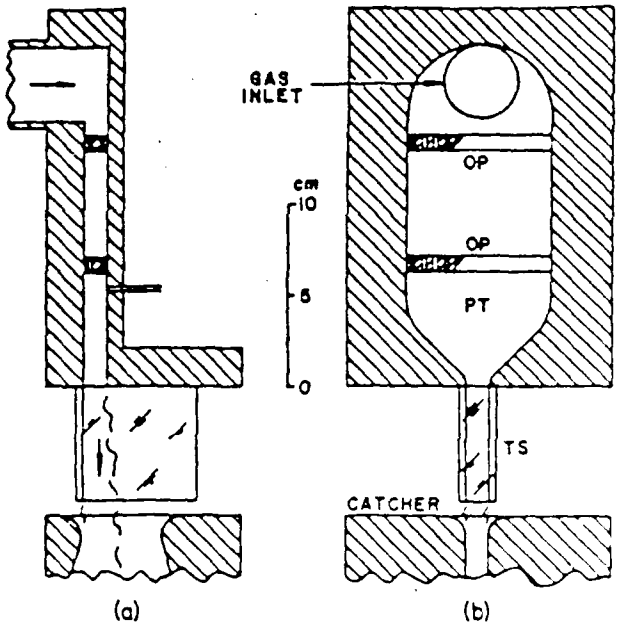

Fig. 2. Nozzle and test section. OP are orifice plates, PT is the pressure tap, and TS is the test section.

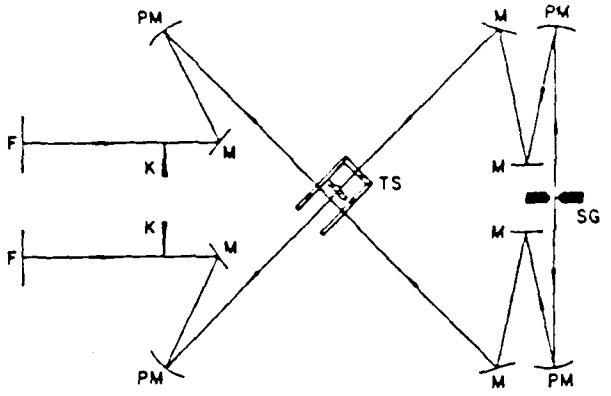

Fig. 3. Two direction schlieren system. SG is the spark gap, M are plane mirrors, PM are parabolic mirrors, TS is the test section, K are knife edges and F are photographic plates.

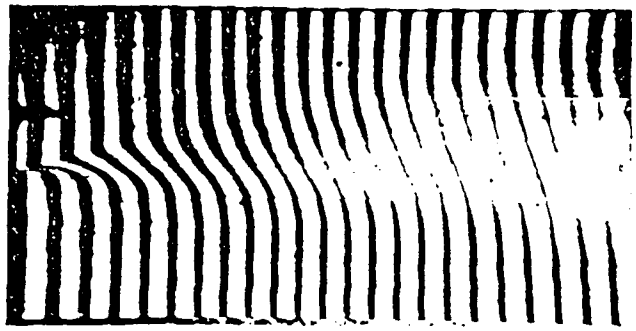

Fig. 4. Long exposure interferogram at M_1=0.32, λ_ρ=1.07. Gas jet is on bottom. Flow is from left to right. $Re_{x,max}=2.6 \times 10^5$.

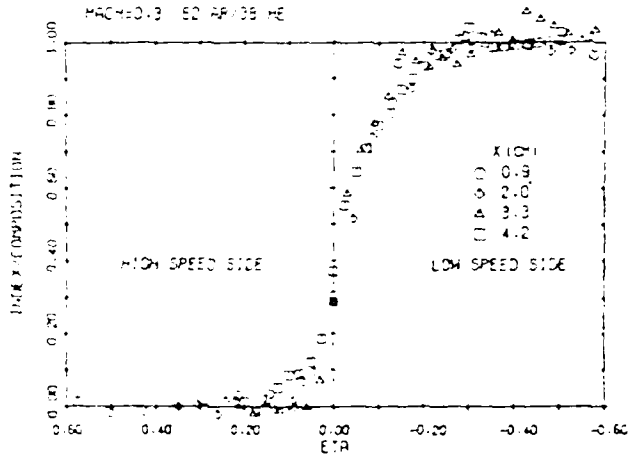

Fig. 5. Nondimensional index profiles of M=0.32, λ_ρ=1.07 jet. x is the distance downstream of the nozzle exit.

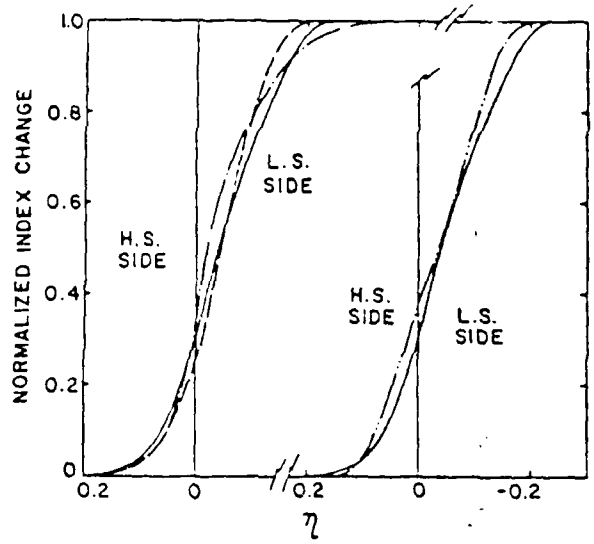

Fig. 6. Nondimensional index profiles. Lefthand graph shows our data for various Mach numbers: M=0.1 (solid line), M=0.3 (dash-dot line) and M=0.6 (dashed line). Righthand graph compares our M=0.1 data (solid line) with data from Fiedler[5] (dash-double dot line).

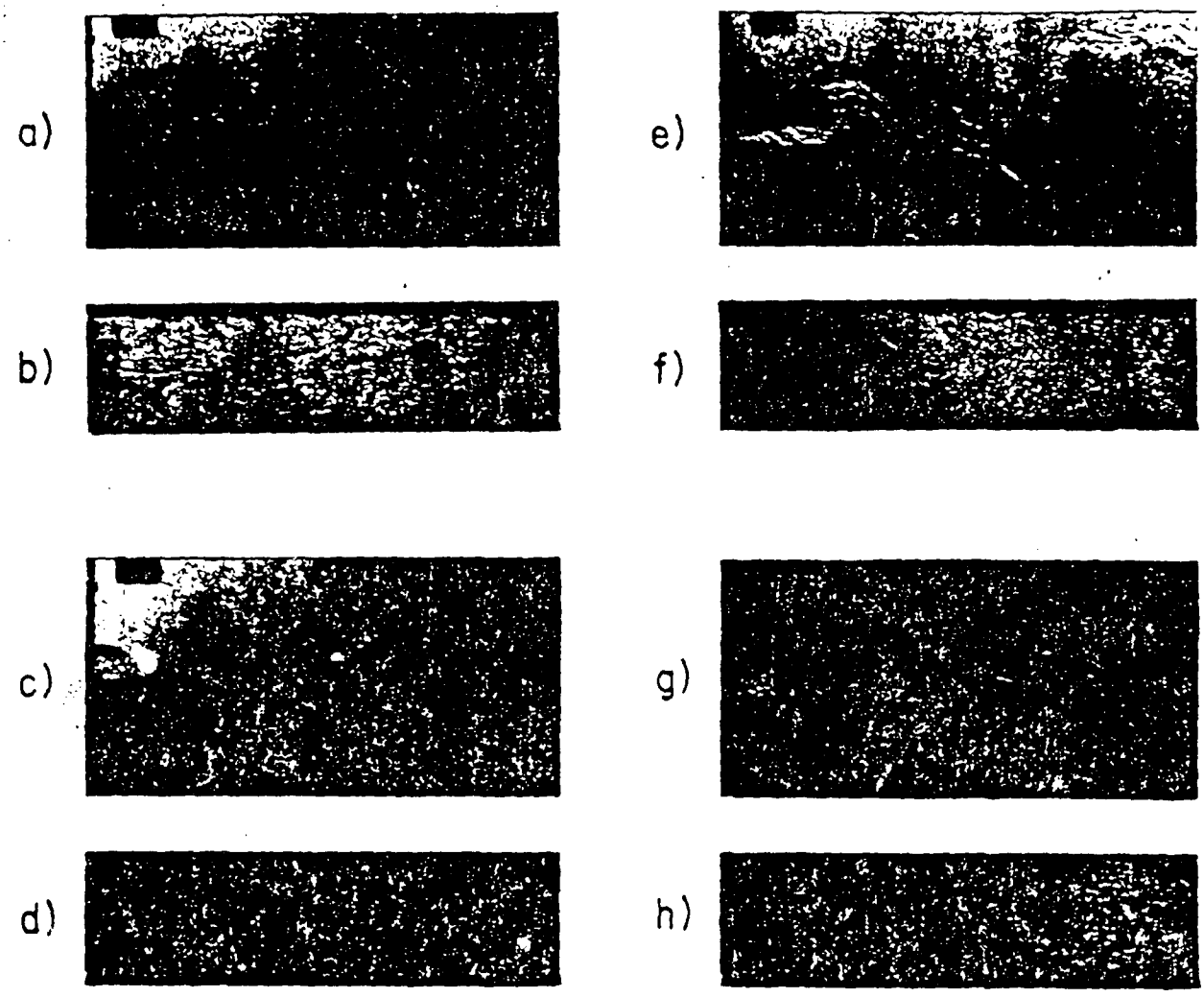

Fig. 7. Two direction schlieren photographs. The upper photograph of each pair was taken looking parallel to the shear layer and the lower photograph was taken looking normal to the shear layer. a) and b): M=0.11, λ_ρ=3.2, c) and d): M=.57, λ_ρ=2.9, e) and f): M=0.13, λ_ρ=0.66, and g) and h): M=0.69, λ_ρ=0.60.

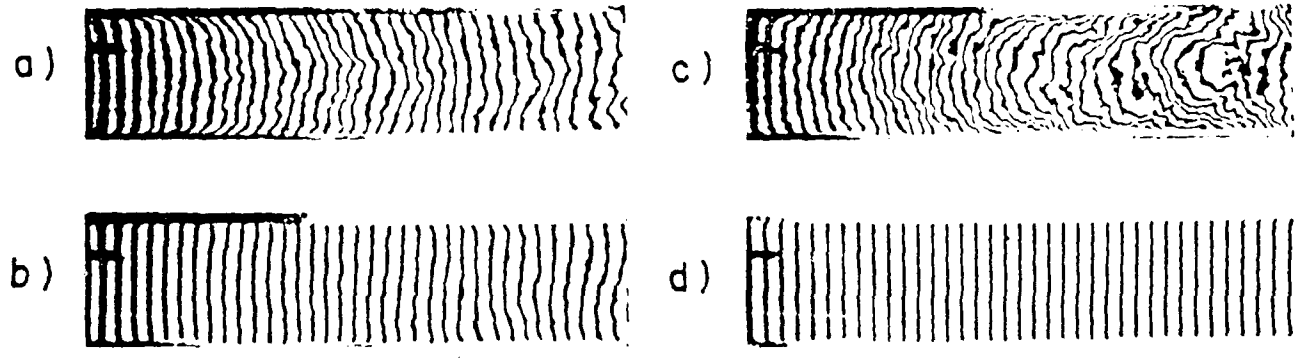

Fig. 8. Beam degradation interferograms taken at M_1=0.6. Flow is from left to right. Gas mixtures are a) CO_2, b) 38He/62Ar, c) He and d) tare.

Appendix

Determination of the Density Profile in the Shear Layer via Computer Processing

The density profile in the shear layer may be determined directly by means of digital optical readout and processing by a computer. As an interim step to a more sophisticated system yet to be developed, we are using a Microneye camera with a 256×128 pixel format and Apple II computer. In this approach, a photograph of the shear layer from the Mach-Zehnder interferometer is used as the source of information. Using the Microneye computer program, the photograph can be displayed on the monitor or printed using a dot matrix printer with graphics capability as shown in Fig. A(1). Due to turbulence in the flow, the fringes in the shear layer are not clear enough. Therefore, many pictures of the same object with different light levels (40% to 60%) were taken, and summed in the computer memory. This was done in an effort to enhance contrast levels. (The information at each point on the screen is translated into binary data as 0 (bright dot) and 1 (dark dot) and summed appropriately for 5 pictures.) The central location of each fringe is determined according to the location and width of the maximum value. The dots shown in Fig. A(1) are the fringe center locations drawn by the computer. The tare picture is treated in the same way, but only one picture needs to be taken because the fringes are distinct everywhere.

The number of the fringes in each picture is then counted along 15 horizontal lines. The density in the flow field along this sampling line is then calculated. On each line, the number of fringes at that position is calculated and the optical density obtained by using

$$(\beta\rho) = \frac{\lambda}{L}(NF - NT) + (\beta\rho)_a$$

where λ = wavelength of laser beam,
L = optical path length,
$\beta\rho$ = optical density of test gas mixtures
$(\beta\rho)_a$ = optical density of air,
NF = fringe number of test picture, and
NT = fringe number of tare picture.

Connecting the density value at each point vertically, a density profile picture is obtained. Manual correction of the data is necessary to get accurate values of $\beta\rho$. One of the results of the calculation on Fig. A(1) is shown in Fig. A(2). However, this method was not used in the reduction of the interferograms presented in this paper, since the method is not yet perfected.

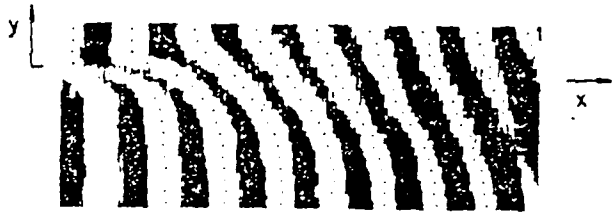

A1

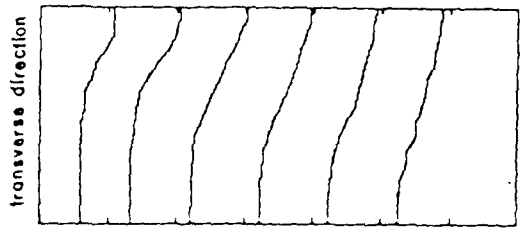

A2

Fig. A1. Digitized interferogram at M_1=0.32.
Fig. A2. Optical density profiles ($\beta\rho$) at six stations downstream of the nozzle exit.

Inst. Phys. Conf. Ser. No. 72
Paper presented at 5th GCL Symp., Oxford, 20–24 August 1984

A study of inhomogeneous shear layers and their effect on laser beam degradation

Walter H. Christiansen, Hamid Johari, D.W. Bogdanoff

Department of Aeronautics and Astronautics, University of Washington
Seattle, Washington 98195, U.S.A.

Abstract. Optical properties of two-dimensional, subsonic shear layers with zero velocity ratio have been investigated. Measurements of shear layer growth rates and laser beam degradation for propagation normal to the turbulent interface are presented. The shear layer growth rates were found to decrease with increasing Mach number. Interferograms taken normal to the shear layer show that the beam degradation is a function of the index of refraction difference across the layer.

1. Introduction

Shear layers and wakes occur in the resonators of many high power lasers. The extraction of power usually involves passing the beam through interfaces which often involve dissimilar gases of different optical properties. Shear layers are also an important feature of aerodynamic windows. While a number of investigations (Legner et al 1978, Vu et al 1980) of the optical properties of this flow have been carried out, additional study is warranted to cover a wider range of experimental conditions.

The fluid dynamics and gas optical properties of single two-dimensional shear layers have been studied at Mach numbers and Reynolds numbers appropriate for lasers. Experimentally this involves a systematic investigation through independent control of density ratio and compressibility effects of the free jets. This is usually accomplished by using jets of various helium and argon mixtures. Of importance is the examination of compressible shear layers accompanying these jets for evidence of coherent, large scale vortical structures, since such large scale structures are more troublesome optically than a random turbulent field.

Shear layer spreading rates were measured using long-exposure interferograms and schlieren photographs. These tests were done at Mach numbers of 0.1, 0.6 and 0.9 with various density ratios. These growth rates are compared with the literature. Interferograms using a ruby laser beam parallel and perpendicular to the shear layer have been taken also. The photographs provide phase error data which can be used to determine the scale and amplitude of the refractive index perturbations in the layer.

2. Experimental Setup

This investigation is focused on zero velocity ratio shear layers in which a two-dimensional symmetric nozzle with a 1.4 cm square exit was employed. Free stream turbulence is reduced by two orifice plates. The nozzle has a 6:1 area contraction with steep (45°) sidewalls to minimize boundary layer growth. The momentum thickness, θ, at the exit of nozzle was calculated to be 0.0027 cm for $M_1 = 0.1$. The test section is formed from three flat

plates of optical glass set up to be a continuation of three walls of the nozzle. The open fourth side allows the room air to mix with the nozzle exit flow. The test section is 7.5 cm long. Jets of various helium and argon mixtures permit variations of density ratio at different flow conditions. The Reynolds number, based on the nozzle exit dimension, ranges from $3.1(10^4)$ to $3.3(10^5)$ for a mixture with $\lambda_\rho = 1$ and $M_1 = 0.1$ to 0.9, respectively. The gases tested are He, N_2, CO_2 and two mixtures consisting of 86 He/14 Ar and 38 He/62 Ar by volume.

Long exposure interferograms were taken parallel to the shear layer with a Mach-Zehnder interferometer. Two different laser light sources are used with the interferometer. Long exposure photographs are taken using a 1 mW He-Ne laser as the light source. Optical quality data were obtained using short exposure interferograms taken normal to the shear layer. A Q-switched ruby laser was used as the light source.

3. Spreading Rate Measurements

Long exposure interferograms were used to measure the shear layer spreading rate. An exposure time of about 0.1 sec was used to give proper time-averaging. The mean growth rate of the index of refraction profiles of the shear layer were measured by counting the fringe shifts. Fig. 1 is an interferogram for a gas mixture (38 He/62 Ar) having a density equal to that of air at room temperature at $M_1 = 0.3$. The gas mixture is on the left portion of the photograph. Other interferograms were taken at Mach numbers of 0.1 and 0.6. Self-similar profiles were obtained using a computer program minimizing the mean square error of this profile. Fig. 2 shows refractive index profiles plotted in non-dimensional coordinates for the interferogram shown in Fig. 1. The transverse coordinate is η, defined as $\eta = y/(x-x_o)$. The vertical axis of Fig. 2, refers to refractive index

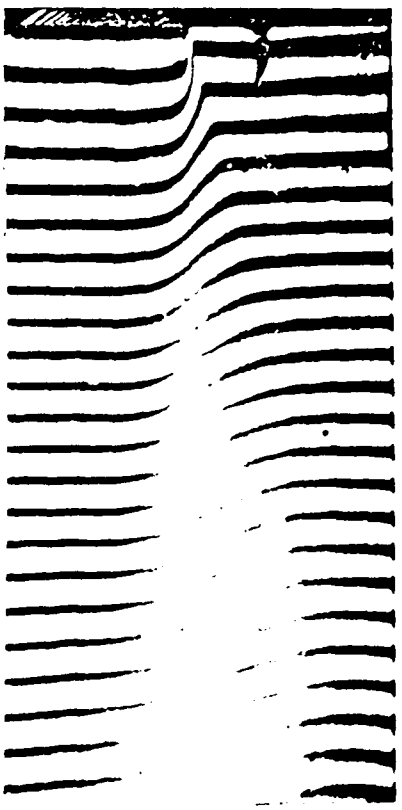

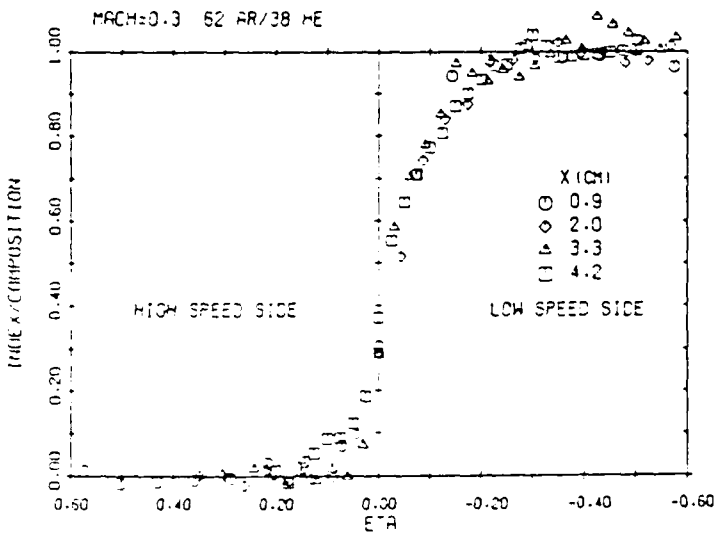

Fig. 1. (left) Long exposure interferogram at M_1=0.3. Gas jet is at left. Flow is from top to bottom.

Fig. 2. (right) Nondimensional index profile of this interferogram. x is the distance downstream of the nozzle exit.

variation Δn inside the shear layer non-dimensionalized by the difference of the index between the free stream and ambient air. The downstream position of each data set is also shown in the figure.

Fig. 3 shows the best fit curve for three mean index profiles and Fiedler's (1974) mean temperature data. The right hand portion of the graph shows the comparison between Fiedler's curve and the $M_1 = 0.1$ profile. The two curves agree reasonably well. The left hand side of Fig. 3 presents a comparison among $M_1 = 0.1$, 0.3, and 0.6 profiles. Note that the $M_1 = 0.6$ profile has a smaller growth rate than $M_1 = 0.1$. A comparison among this data and that of Fielder (1974) is presented in Table 1. For this data λ_ρ is nearly one. The Reynolds number of the flow is based on free stream properties and the maximum tested length of the shear layer, x_{max}. According to Bradshaw (1966) the detailed turbulence structure of a free shear layer becomes self-similar at distances greater than 1000 momentum thicknesses (calculated at the nozzle exit). The shear layer thickness is Δn which was defined by the slope of a straight line passing through the non-dimensional points $\Delta n = 0.2$ and $\Delta n = 0.8$.

Author	M_1	$Re_{x,max}$	$\frac{x_{max}}{\xi}$	Δn
Fiedler	0.02	4.0×10^5	1400	0.26
This work	0.12	8.4×10^4	1400	0.28
"	0.32	2.6×10^5	2600	0.20
"	0.58	2.8×10^5	1900	0.20

Table 1. Comparison of index profiles.

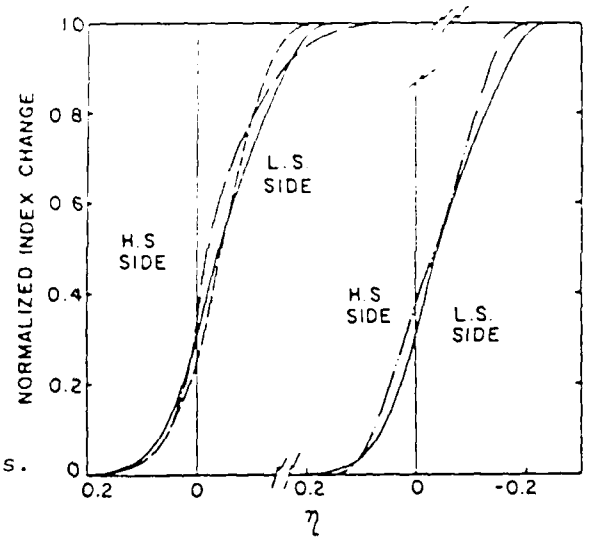

Fig. 3. Nondimensional index profiles. Lefthand graph shows the data for various Mach numbers: M_1=0.1 (solid line), M_1=0.3 (dash-dot line) and M_1=0.6 (dashed line). Righthand graph compares the M_1=0.1 data (solid line) with data from Fiedler (dash-double dot line).

4. Schlieren Observations

Time averaged schlieren photographs were taken parallel to the shear layer for $M_1 = 0.1$, 0.6 and 0.9. (Short exposure results are detailed in Johari et al 1984). The visual spreading rates of the shear layers, $\Delta n_{vis} = \Delta y_{vis}/x$, were read off the photographs. The sensitivity of the schlieren system was insufficient to give reasonable estimates of the spreading rates for those gases which were nearly index-matched, i.e., 38He/62Ar and N_2. The data from the other tested gases is shown in Fig. 4. Both Mach number and density ratio effects are evident. The shear layer spreading rates at $M_1 = 0.9$ are about 0.7 times those at $M_1 = 0.1$. This ratio is nearly the same reduction as predicted by Bogdanoff (1983). For the $M_1 = 0.9$ data, the reductions in shear layer spreading rates with increasing M_1 are consistent with a compressibility effect, while the $M_1 = 0.6$ data cannot be completely explained as compressibility effects. The spreading rates with $\lambda_\rho = 0.61$ are about 0.7 times the rates at $\lambda_\rho = 6.5$.

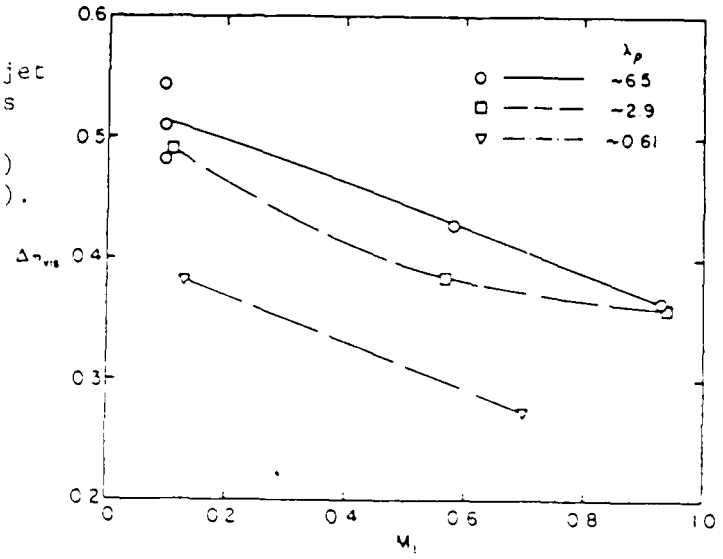

Fig. 4. The visual spreading rates of the shear layer as a function of the jet Mach number. Gases are He (circles), 86He/14Ar (squares) and CO_2 (triangles).

5. Optical Quality Measurements Normal to the Shear Layer

Stop-action interferograms were taken parallel to the shear layer for various density ratios and Mach numbers. Fig. 5 shows four interferograms taken at M_1 = 0.9 for CO_2, 38He/62Ar, 86He/14Ar, and He. Although the shear layers spreading rates are different, common features are noticed. Large scale structures appear to exist in all cases. Second, there are

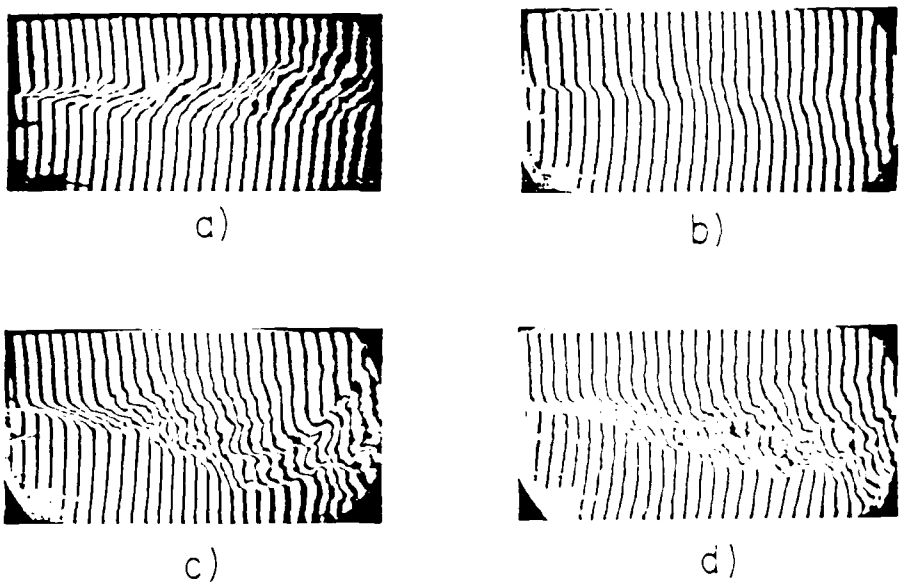

Fig. 5. Stop-action interferograms viewing the shear layer spreading at M_1=0.9. Flow is from left to right. Gas jet is on top. Gases are a) CO_2, b) 38He/62Ar, c) 86He/14Ar and d) He.

regions in the irrotational fluid where disturbances exist next to such structures which imply engulfment of irrotational fluid. Fig. 6 shows interferograms taken normal to the shear layer at $M_1 = 0.6$. The density ratios are 0.60, 0.99, and 6.5 for CO_2, 38 He/62 Ar, and He, respectively. There is a striking difference between the index fluctuations. The index difference between the jet and air at room temperature was lowest for the mixture ($\Delta n = 7.7 \times 10^{-5}$) and highest for He ($\Delta n = 2.35 \times 10^{-4}$).

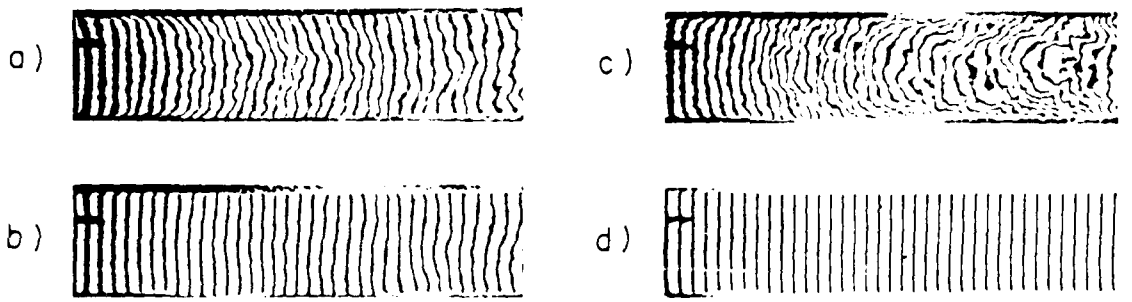

Fig. 6. Beam degradation interferograms taken at $M_1 = 0.6$. Flow is from left to right. Gases are a) CO_2, b) 38He/62Ar, c) He and d) tare.

An important measure of the laser beam degradation is the Strehl ratio or loss of peak far-field intensity caused by the flow field, I/I_o. It is known that for a tilt and focus corrected laser beam that $I/I_o = \exp[-\langle \Delta\phi^2 \rangle]$ where $\langle \Delta\phi^2 \rangle$ is the mean square phase error over the area. If one assumes that the index fluctuations are homogeneous within the shear layer (a poor assumption in view of the evidence for coherent structures in shear layers and the variation of its structure), an estimate of I/I_o can be made. The reduction in far-field intensity due to turbulent fluctuations is given by Sutton (1969) for this case as an exponential function of k, the wavenumber, Λ, the integral scale of the turbulence, L, the shear layer thickness, and $\langle \Delta n^2 \rangle$, the averaged index fluctuation. In inhomogeneous shear layers both variations in the Gladstone-Dale constant, β and ρ can contribute to Δn. To estimate the Strehl ratio one needs to measure or to predict L, Λ, and $\langle \Delta n^2 \rangle$. While this equation is only an approximation for shear layers, an important aspect of the work is to measure these variables for shear layers of interest and to model these results. The phase errors can be correlated with δn across the shear layer.

Each near-field interferogram is digitally read by a Microneye camera and the information is stored using a micro-computer. The central location of each fringe is determined with respect to specific reference lines. The tare interferogram is treated the same way. The net fringe shift is obtained by subtracting the tare from the disturbed fringe pattern. These values are then averaged over an area and finally, the root mean square phase error at the location of reference lines is computed. While the tilt correction has not been removed from this set of measurements, this correction was negligible up to about two nozzle widths downstream. Further downstream, tilt became an important factor; however, at such locations, the flow is not two-dimensional any longer because of wall effects. Another point that should be emphasized is that the results are in terms of the interferometer wavelength (0.6^{0}u). Hence, the phase error for a laser device with a different wavelength should be properly scaled.

Figures 7 and 8 show the effect of density ratio and Mach number on the root mean square phase error at 0.69μ. Fig. 7 represents the phase error as a function of downstream position for a jet of 86He/14Ar at various Mach numbers. The three curves and the values are very similar. The only difference seems to be in the position of peaks and valleys which appears to be a result of passage of nonsteady vortical structure. This feature is more apparent in Fig. 8, where three gases are compared at $M_1 = 0.6$. The root mean square phase error increases in the downstream direction since the shear layer grows. The values of Strehl ratio obtained from the near-field phase error data is comparable to those given by Legner et al (1978) and Vu et al (1980). The experimental results do not agree closely with the theoretical derivation of Sutton (1969), because of the presence of the coherent structures. If we assume that the integral scale of turbulence is of the order of the shear layer thickness, the theoretical prediction agrees roughly with the experimental results.

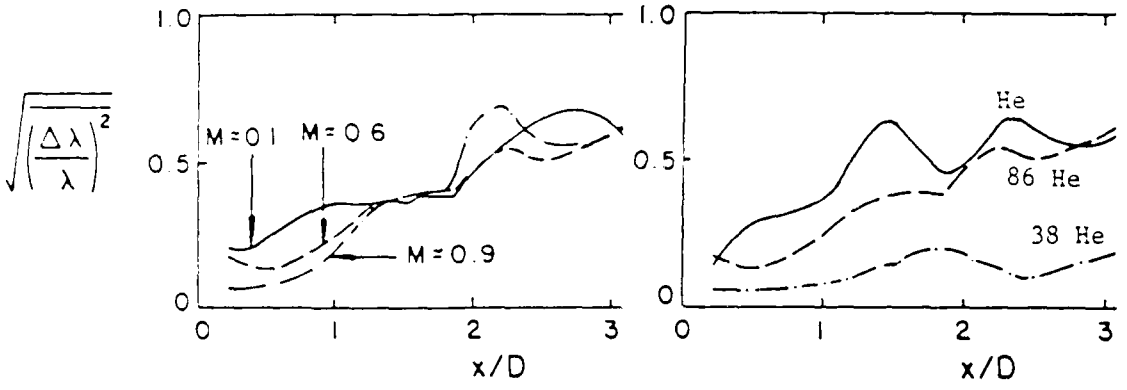

The root mean square phase error as a function of the downstream position. The gas mixture in Fig. 7. (left) is 86He/14Ar. The gases in Fig. 8. are He (solid line), 86He/14Ar (dashed line) and 38He/62Ar (dash-dot line).

In conclusion, a shear layer of matched refractive index produces the least near-field phase error. Large scale vortical structures are very troublesome and seriously degrade the optical quality of flows. The estimated Strehl ratios of the shear layers studied here may be acceptable at infrared wavelengths, but are unacceptable in the visible range.

Acknowledgment. This research was sponsored by the Air Force Office of Scientific Research. The authors also thank Prof. H.T. Chen, a visiting Research Associate, for his reduction of the near-field data.

References

Bogdanoff D W 1983 AIAA J. 21 926
Bradshaw P 1966 J. Fluid Mechanics 26 225
Fiedler H E 1974 Advances in Geophysics (New York: Academic Press) 18A pp. 93-109.
Johari H, Poling H, Chen H T, Bogdanoff D W and Christiansen W H 1984 AIAA paper 84-1622
Legner H H, Otis J H, Theophanis G A and Fienberg R M 1978 AIAA paper 78-71
Sutton G W 1969 AIAA J. 7 1737
Vu B T, Sutton G W, Theophanis G A and Limpaecher R 1980 AIAA paper 80-1414

FAR FIELD OPTICAL PROPERTIES IN COMPRESSIBLE INHOMOGENEOUS SHEAR LAYERS

Thomas C. Blum
University of Washington
Seattle, Washington

Abstract

The time averaged optical properties of inhomogeneous shear layers have been investigated and are reported here. The principal far field measurement used is the Strehl Ratio. That is, the peak far field intensity of a high quality He-Ne laser beam is measured in the far field with and without the shear layer present. Their ratio determines the Strehl Ratio. The initial results of the study provide information for shear layers of CO_2, He and mixtures of He and Ar for M = 0.6. The results are compared to those done previously at low Mach number and are also used with a theoretical expression to investigate the near field phase error in the laser beam. Near field measurements taken previously for spreading rate information are also presented here for completeness.

Introduction

It is known that turbulence and coherent structure occur in shear layers, even at modest Reynold's number [1]. The performance of optical systems can be severely degraded when laser beams or images are passed through inhomogeneous shear layers. Optical properties of shear layers is a current topic of research with a wide range of applications which include high powered lasers, optical imaging systems, and proposed defense systems.

Computer coupled image processing systems have greatly facilitated the type of investigation reported on here. Images taken by a 256 x 256 array of photo diodes can be stored and manipulated easily by such a system and accordingly much of what is presented here is in the form of computer output.

Background

A shear layer is the region formed by two flows of differing velocities characterized by turbulence and large scale structures [1]. Fig. 1 shows the shear layer formed by a CO_2 jet exhausting into still air. The width of the shear layer is typically defined by some percentage of change of a relevant quantity from the free stream values. This report uses the 90% - 10% normalized index of refraction change $((n_{jet} - n) / (n_{jet} - n_{air}))$ definition. Other thicknesses may be defined by velocity, temperature, or other fluctuations in the layer. Another parameter which is often defined for shear layers is the integral turbulence scale, or macro scale which is the mean size of large scale eddies that form distinct "packets of turbulence" in the shear layer. The nonuniform mixing of the two dissimilar fluids gives rise to these packets which are the source of refractive index and density fluctuations across the shear layer.

Theory

The index of refraction for a gas can be found from the following expression [2]:

$$n = 1 + \beta \frac{\rho}{\rho_s} \qquad (1)$$

where n is the index of refraction, β is the Gladstone-Dale constant for a given species, ρ is the gas density, and ρ_s is the gas density at standard conditions. The index of refraction for a uniform gas mixture is found by using the Gladstone-Dale constant for the mixture:

$$\beta_m = \beta_1 V_1 + \beta_2 V_2 + \ldots + \beta_n V_n \qquad (2)$$

where β_n is the Gladstone-Dale constant of the nth species and V_n is the volume fraction of the nth species.

The optical data in this report are based on a reference beam formed by plane waves incident on a circular aperture. The resulting far field diffraction pattern is the well known Airy pattern which consists of a central bright spot known as the Airy disk surrounded by concentric subsidiary maxima. (For reference, see Born and Wolf, Principles of Optics, pp 395-396). The power in the beam within a radius r is found by integrating the far field intensity pattern over the area. For the reference configuration, the power versus nondimensional radius is given in figure 2 [3] and will be used later to compare with the experimental data. The nondimensional radius used in figure 3 is given by [3]

$$x = kaw \qquad (3)$$

where k is the wave number, a is the aperture diameter, and w is the radial coordinate of any point in the aperture normalized by the aperture to image plane distance.

The Strehl Ratio which is the peak far field intensity ratio with and without flow, can be found by differentiating the power distribution with respect to r as r goes to zero. If Power in fig. 2 is given by

$$P = 2\pi \int_0^r I(\xi)\, d\xi$$

for the Airy pattern, then the intensity is given by

$$I = \frac{d}{2\pi r dr} \int_0^r 2\pi I(\xi) d\xi = \frac{1}{2\pi r} \frac{dP}{dr} \qquad (4)$$

The Strehl Ratio is thus found by taking the ratio of eq. (4) with and without flow as r goes to zero:

$$\frac{I}{I_o} = \lim_{r \to o} \left[\left(\frac{d\sigma}{dr}\right)_{flow} / \left(\frac{d\sigma}{dr}\right)_{ref} \right] \qquad (5)$$

Eqs. (4) and (5) are exact only for intensity patterns that are circular; however they give a reasonable approximation for small dependence on angular position. For noncircular patterns which usually occur only for highly degraded beams an effective Strehl Ratio may be defined as the power remaining within the principal maximum of the reference pattern normalized by the power in the principal maximum of the reference pattern:

$$S_e = \frac{\left[\int_o^r \int_o^{2\pi} I(r,\theta) dr d\theta \right]_{flow}}{\left[\int_o^r \int_o^{2\pi} I(r,\theta) dr d\theta \right]_{ref}} \qquad (6)$$

Sutton has derived an alternative expression for the Strehl Ratio produced by a homogeneous turbulence zone [4]:

$$\frac{I}{I_o} = \exp \left[-2K^2 \langle \Delta n^{-2} \rangle \Lambda L \right] \qquad (7)$$

where K is the wave number, Λ is the integral turbulence scale, L is the width of the zone, and $\langle \Delta n^{-2} \rangle$ is the mean square refractive index change through the zone. The expression in brackets in eq. (7) is the mean square phase error in the near field [5]. If Λ is approximated as L times a constant [5] and $\langle \Delta n^{-2} \rangle$ is taken to be proportional to the square of the refractive index difference across the layer, Δn, eq. (7) has the form

$$\frac{I}{I_o} = \exp \left[-A \Delta n^2 L^2 \right] \qquad (8)$$

where A includes all constants of proportionality (for clarity, A will be defined as $2K^2 \alpha^2 C$ where α^2 is given by $\langle \Delta n^{-2} \rangle = \alpha^2 \Delta n^2$ and C is given by $L = \Lambda C$). This expression which is for a tilt and focus corrected beam passing through a homogeneous turbulence zone, will be used to evaluate A when the Strehl Ratio, Δn, and L are known. The assumption that $\langle \Delta n^{-2} \rangle$ is proportional to Δn^2 is good only while compressibility effects are small since compressible layers that are index matched are known to give Strehl Ratios less than 1 [6].

Experimental Setup

The shear layer was formed by exhausting a subsonic nozzle 1.4 cm on a side into still air. The nozzle which had a 7 to 1 contraction ratio was surrounded on three sides by optical glass which formed the test section. The nozzle was designed to minimize boundary layer growth and a 12" aluminum section was added above the test section to inhibit suction and entrainment downstream of the test section.

The far field measurements were made by passing a beam of laser light through the shear layer parallel to it. The optics system consisted of a high quality He-Ne laser, a pin-hole spatial filter, two telescopes, various filters, masks and a ccd camera with a 256x256 array of photo-diodes. The system was arranged on two aluminum rails as shown in fig. 3. A twelve volt light bulb was used to provide a flat field in order to resolve parts of the signal from the random shot noise produced by the camera. The signal to noise ratio of the camera was about 50:1.

The camera was connected to an imaging system which was coupled to a micro-computer. The camera provided the imaging system with an analog signal which was then digitized and stored in an array and could be easily manipulated by a FORTRAN code written for the experiment.

The data, obtained for CO_2, He, Ar, and mixtures of He and Ar, were taken at standard conditions. The near field data which provided spreading rate information were found using Mach-Zender and shear interferometers.

Shear Layer Thickness Calculation

The thickness L of the shear layer at any downstream location is determined from $\Delta\eta$, the spreading rate parameter ($\Delta\eta = L/(X-X_o)$). Values of $\Delta\eta$ for the shear layers were found in the laboratory concurrently with this experiment [7] and are given in table 1. X_o is the virtual origin of the shear layer and is slightly up stream of the nozzle exit. This effective displacement of shear layer origin is due to the boundary layer at the nozzle exit. As stated earlier, the 90% - 10% normalized refractive index change definition is used to compute $\Delta\eta$. $\Delta\eta$ was found using interferometric techniques.

Far Field Measurements

As was mentioned earlier, the classical Airy intensity pattern is the reference configuration used in this experiment. Figure 5 shows the pseudo 3-D result for the .5 cm aperture. Each line in fig. 4 represents the digitized signal from the corresponding line of pixels in the camera array. Every 16th line is plotted. The plots are shown from an intermediate perspective so that intensity in three directions can be shown. Note the appearance of the first ring. Subsequent ring maxima are completely lost in the random noise of the camera. Fig. 5 shows the normalized power distribution for fig. 4 which is compared to the theoretical result. Both curves are of similar shape; the reference curve, however, rises faster and approaches its maximum value faster. This shift is a result of the fact that the normalization factor which is the total power in the incident beam is too small due to diffraction off of the array. When scaled by an appropriate factor (taken to be the amount of power within the dark ring that surrounds the last discernable bright ring), the two curves coincide well up to that particular dark ring (see fig. 6).

The time averaged results for a typical experiment are shown in figs. 7 and 8. Fig. 7 is the intensity pattern for 62% He at 1.0 cm downstream with a 0.5 cm aperture. The power distribution and Strehl Ratio calculation for 62% He are shown in fig. 8. The third curve is the tare distribution. The decrease in power near the end is the result of light being scattered off the array and is not expected theoretically. The presence of noise is also seen past the second dark ring which shows the limits of the ccd camera. The Strehl Ratio is computed using a numerical approximation to eq.(5). By calculating the Strehl Ratio from the integral of the intensity pattern, error is reduced by the averaging effect of the integral. However, finding the ratio between the maximum pixels of the tare and the run gives good agreement in most cases. The Strehl Ratio results for five gases, two beam diameters (0.5 and 1.0 cm), and two downstream locations (1.0 cm and 2.0 cm) are given in Table 2. The results are for a free stream Mach number of 0.6 and were found from images with a 0.1 second exposure. Strehl Ratios are higher for smaller beam diameter which on the basis of homogeneous turbulence is expected [4]. Reduction in Strehl Ratio for 1.0 cm beam diameter may also be due to wall effects which create large phase errors in the outer portions of the beam [5]. As the absolute value of the refractive index difference increases, the Strehl Ratio decreases. This was expected. The decrease in Strehl Ratio with downstream distance may be explained by several effects. From eq. (5) the Strehl Ratio is expected to decrease as thickness increases. The Strehl Ratio is also strongly dependent on , the macro scale, which increases with thickness [8] and thus greater degradation is expected downstream. Finally, wall effects are more pronounced downstream and thus larger phase errors occur. The results of Table 2 can be compared with similar and earlier results by Higgins [9] (Table 3) for M = 0.1 with interesting changes occurring. As Mach number is increased, many factors which can improve or degrade the image occur. For instance, for all mixtures, the refractive index tends towards that for air at room conditions which reduces the phase error. The shear layer thickness decreases at higher Mach number which also reduces the phase error. An increase in Reynold's Number would be expected to increase phase error due to higher turbulence intensity. Table 2 and 3 show an increase in Strehl Ratio for all cased at M = 0.6 which indicates the first two effects are more important in this range (compressibility effects at higher Mach number may cause larger refractive index fluctuations which seriously degrade the beam [6]). The calculated error values shown in Table 2 are based on estimates of camera noise, fluctuation in laser background illumination with time and changes in the shear layer from run to run. Smaller values of Strehl Ratio refer to those cases where large phase errors have moved large portions of the beam in the far field such that the method of computing the Strehl Ratio out here may not be valid. Table 4 shows values of effective Power Ratio for these cases.

Fig. 12 is a plot of Strehl Ratio versus $(\Delta n L)^2$ on a log scale. The results for the 0.5 cm diameter beam are nearly straight lines (except for CO_2) which indicate the parameter A in eq. (8) is a constant over this range of $(\Delta n L)^2$. The behavior of CO_2 can not be explained theoretically and is presumed to be in error. It is probable that the shear layer for CO_2 is too thick which decreases the Strehl Ratio and shifts it to the right in fig. (12). The results for 1.0 cm diameter beams are more troublesome and may be in error due to reasons discussed earlier. Fig. 13 is a plot of the parameter $A^*(A/2k^2)$ which is found from eq. (8) versus density ratio and ignoring CO_2 again shows the result that A varies little over the range of gases for the 0.5 cm case. Eq. (7) is derived for homogeneous turbulence and is applied to the present results out of necessity. Therefore, an inherent error in the results of figs. 10 and 11 results due to the presence of coherent structure in shear layers which are inhomogeneous by nature and may cause tilt and focus errors which are not accounted for in eq. (8). However, if the shape of the reference configuration is not changed drastically, the tilt can be effectively corrected for in the data be carrying out the integration of the intensity pattern from the new intensity centroid location. This effective correction is less valid for the 1.0 cm beam at 2.0 cm downstream and for some of the large refractive index change mixtures which have severely altered images. However, it may also be noted that the shear layer becomes more homogeneous downstream as mixing occurs. The error in A may be estimated by differentiating eq. (8) and is found to depend inversely on $(\Delta n L)$ and directly on the uncertainty in Strehl Ratio. Therefore, even when the error in Strehl Ratio is small, large errors may result in A when $(\Delta n L)$ is small. The constant C in A that relates thickness to integral turbulence scale has been determined by other researchers and is approximately 0.25 [8]. Eliminating this factor from A, the constant α^2 relating Δn to mean square refractive index fluctuations may be determined. Table 5 shows α for a number of gases. The data fall into the range found previously by others [6]. Finally, a word should be said about previous and current attempts of modeling phase degradation by shear layers with homogeneous turbulence results. The data presented here agree with theory and previous experiments. This agreement, in some cases may be strictly fortuitous. That is the instantaneous results due to coherent structure may be quite different from those predicted by eq. (7) and only when they are time averaged do they agree. For example, it has been suggested [10] that the shear layer may refract the beam back and forth with a high enough frequency that the time averaged effect is a smeared intensity distribution similar to that produced by random turbulence. Fig. 12 shows the far field intensity distribution for 62% He at M = 0.6. Clearly, this is not the pattern produced by homogeneous turbulence and may be partially explained by large scale effects.

Conclusion

The time averaged Strehl Ratios for various gases and beam diameters were found experimentally. Computer images provided other information such as power and intensity distributions in the far field. The Strehl Ratio results were used with a theoretical expression for homogeneous turbulence so that the near field phase error could be investigated and perhaps predicted for some cases. The results agreed reasonably well with those found by other researchers, especially at the smaller beam diameter. Image degradation increased with refractive index difference, downstream distance, and increasing beam diameter. The time averaged effects of large scale structures in shear layers are significant but there is reason to believe that instantaneous results may differ and should be investigated. Finally, the use of a computer coupled image processing system is highly recommended for use in taking, storing, and manipulating data.

Acknowledgments

The author would like to thank A. Westpnal and D. Higgins for writing much of the software used to manipulate the data.

References

1. Brown, G.L. and Roshko, A. "On Density Effects and Large Structure in Turbulent Mixing Layers", Journal of Fluid Mechanics, Vol. 64, Part 4, 1974, pp 775-816.

2. Liepmann, H.W. and Roshko, A. "Methods of Measurement", Elements of Gasdynamics, Wiley and Sons, New York, 1954, pp. 154.

3. Born, M. and Wolf, E. Principles of Optics, 3rd Ed., Pergamon Press, Oxford, 1964, pp 395-398.

4. Sutton, G. "Effect of Turbulent Fluctuations in an Optically Active Fluid Medium", AIAA Journal, Vol. 7, No. 9, Sept. 1969, pp 1737-1743.

5. Johari, H., Christiansen, W., and Bogdanoff, D., "A Study of Inhomogeneous Shear Layers and Their Effects on Laser Beam Degradation", 5th GCL Symposium, Oxford, August 1984.

6. Vu, B.T., Sutton, G., Theophanis, G. and Limpaecher, R. "Laser Beam Degradation Through Optically Turbulent Mixing Layers", AIAA Paper No. 80-1414, AIAA 13th Fluid & Plasma dynamics Conference, July 1980.

7. Tsai, Y., graduate student, and Yu, G., Research Assistant, unpublished data, University of Washington, Aerospace and Energetics Research Laboratory, Spring 1986.

8. Batt, R.G. "Turbulent Mixing of Passive and Chemically Reacting species in a Low-Speed shear Layer", Journal of Fluid Mechanics, Vol. 82, Part 1, 1977, pp 53-95.

9. Higgins, D., graduate student, unpublished data, University of Washington, Aerospace and Energetics Research Laboratory, Fall 1985.

10. Christiansen, W., Professor of Aeronautics and Astronautics, University of Washington, Seattle, Discussions, Spring 1986.

TABLE 1 Spreading Rates for Shear Layers

	86% He	62% He	38% He	CO_2
Δn	0.258	0.224	0.207	0.209
X_o	-0.60	-0.50	-0.42	0.00

Δn is computed for the 90%-10% refractive index change definition of the shear layer and X_o is the virtual origin.

TABLE 2 Strehl Ratios at M = 0.6

0.5 cm Beam Diameter

	He	86% He	62% He	38% He	CO_2
d = 1.0 cm	0.64 ± .01	0.77 ± .015	0.93 ± .01	0.98 ± .01	.88 ± .01
d = 2.0 cm	- - -	0.39 ± .015	.69 ± .01	.88 ± .01	.49 ± .02

1.0 cm Beam Diameter

	He	86% He	62% He	38% He	CO_2
d = 1.0 cm	0.18 ± .02	.56 ± .02	0.89 ± .01	0.85 ± .02	0.72 ± .01
d = 2.0 cm	- - -	0.15* ± .01	0.39* ± .02	0.73 ± .01	0.18* ± .02

d refers to downstream distance from nozzle exit

TABLE 3 Strehl Ratios at M = 0.1

0.5 cm Beam Diameter

	He	62% He	38% He	CO_2
d = 1.0 cm	.35	0.6	0.84	0.80
d = 2.0 cm	.21	0.39	0.7	0.45

1.0 cm Beam Diameter

	He	62% He	38% He	CO_2
d = 1.0 cm	.12	- - -	.72	.49
d = 2.0 cm	---	- - -	.35	.20

Results were found by Higgins on same apparatus. Error values were not available.

TABLE 4 Effective Power Ratio at M = 0.6

1.0 cm Beam Diameter, 2.0 cm Downstream

86% He	62% He	CO_2
0.26 ± .02	0.49 ± .01	0.30 ± .01

Effective power ratio is percentage of power in the central maximum that remains after passage through the shear layer.

TABLE 5 α Parameter, M = 0.6

0.5 cm Beam Diameter

	86% He	62% He	38% He	CO_2
d = 1.0 cm	0.089	0.083	0.091	.14
d = 2.0 cm	.10	.11	.13	.17

1.0 cm Beam Diameter

	86% He	62% He	38% He	CO_2
d = 1.0 cm	.13	.13	.26	.23
d = 2.0 cm	.15	.21	.21	.26

α is the constant in $\overline{\Delta n^2} = \alpha \Delta n^2$ that relates the mean square refractive index fluctuations to the square of the refractive index difference across the shear layer.

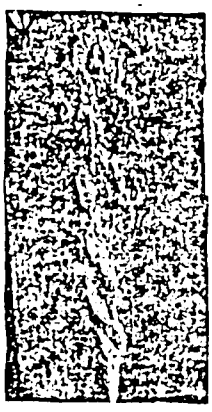

FIGURE 1 Schlieren photograph of shear layer at M=0.6.

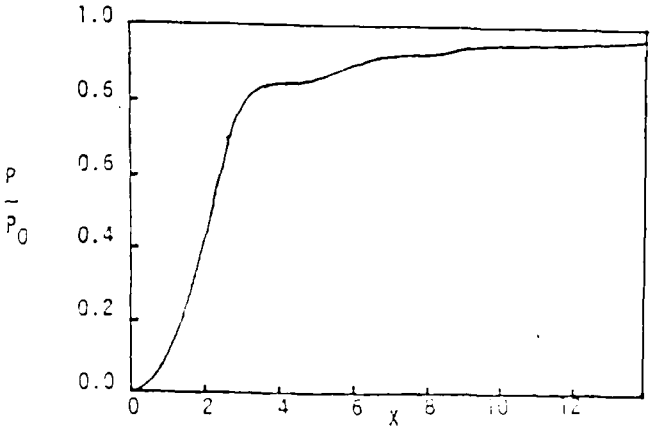

FIGURE 2 Theoretical power distribution for Airy pattern.

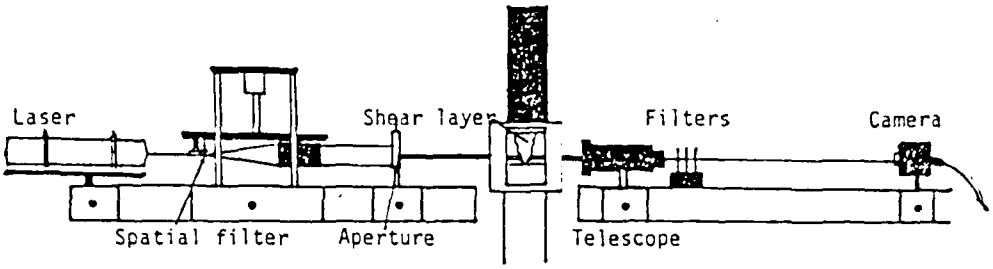

FIGURE 3 Experimental set up.

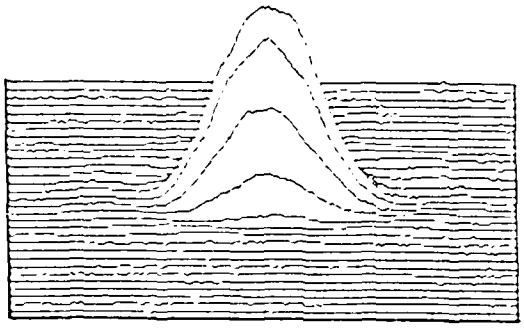

FIGURE 4 Pseudo 3-D intensity pattern for 0.5 cm reference beam. Each line represents digitized output from the corresponding line of pixels in camera array.

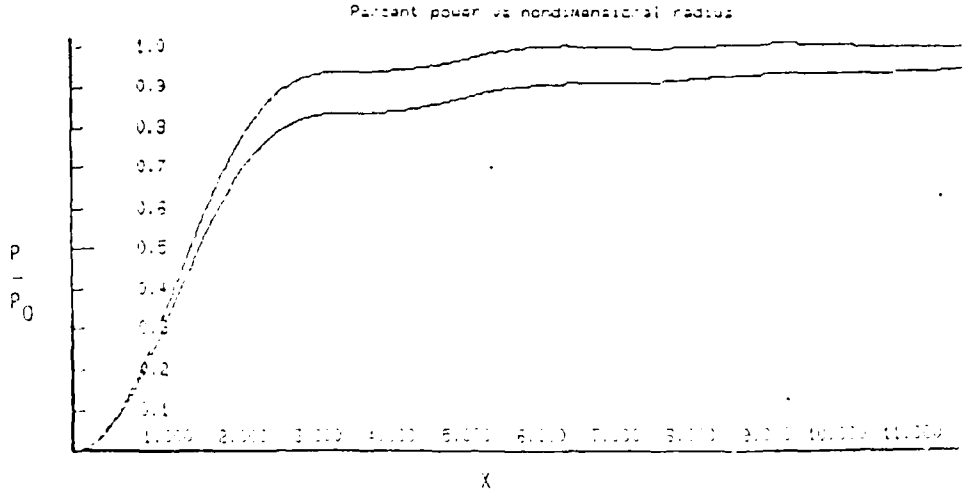

FIGURE 5 Power distribution for pattern shown in Fig. 5 compared to theoretical result.

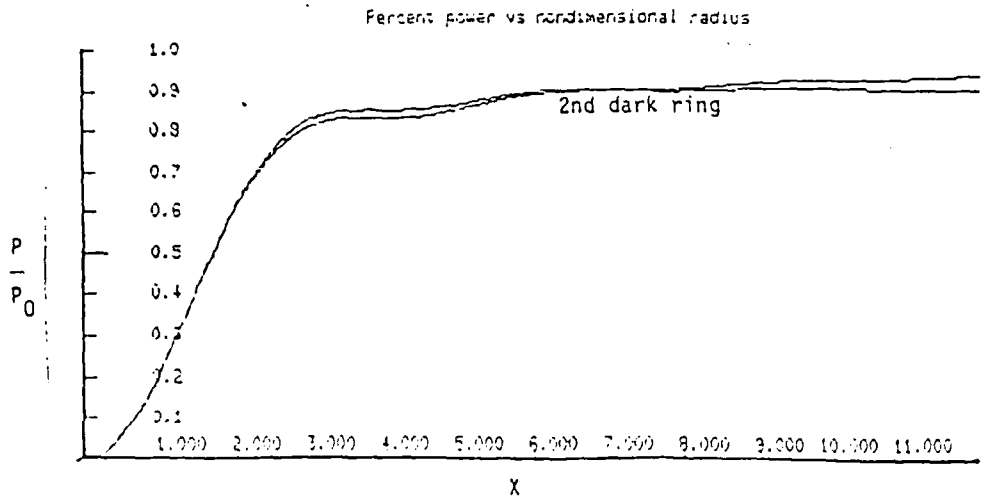

FIGURE 6 Power distribution after scaling by power in 2nd dark ring. Compares well with theoretical up to 2nd dark ring

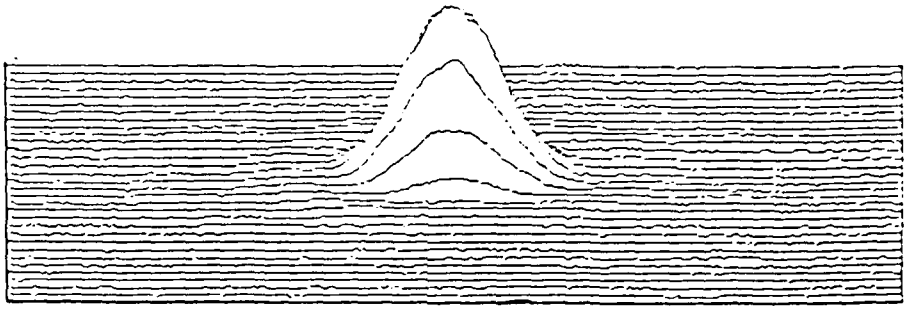

FIGURE 7 Psuedo 3-D intensity pattern for 62% He at M=0.6;0.5cm beam diameter.

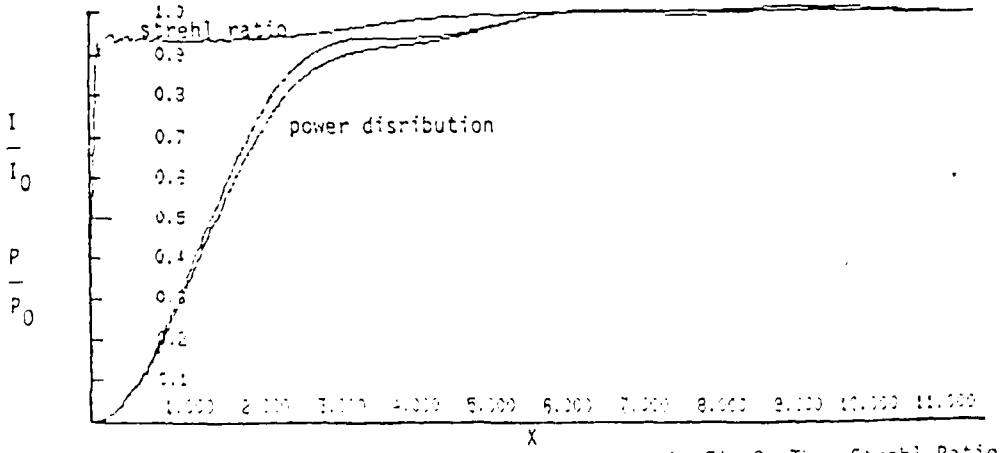

FIGURE 8 Strehl Ratio calculation for pattern in Fig 8. The Strehl Ratio is the value the upper curve approaches as x goes to zero. It is found from the power distributions shown.

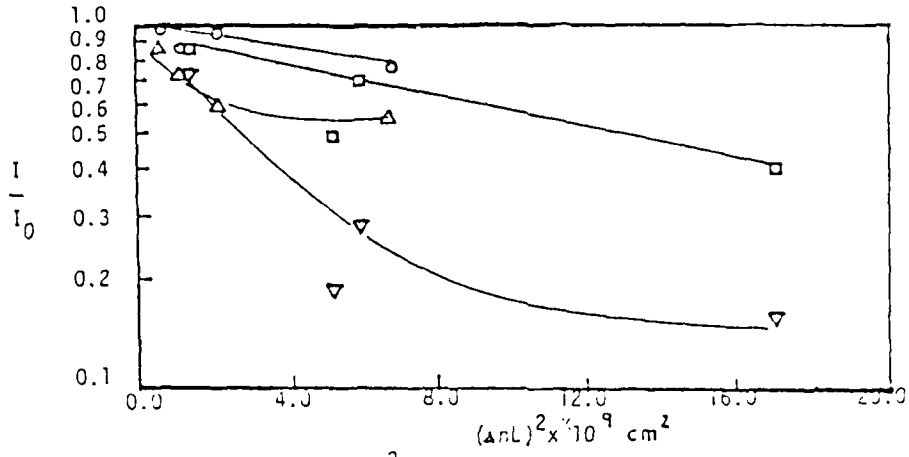

FIGURE 9 Strehl Ratio vs $(\Delta nL)^2$. o-0.5 cm beam,1.0cm downstream,□-0.5cm beam,2.0cm ds,Δ-1.0cm beam,1.0cm ds,▽-1.0cm beam,2.0cm ds.

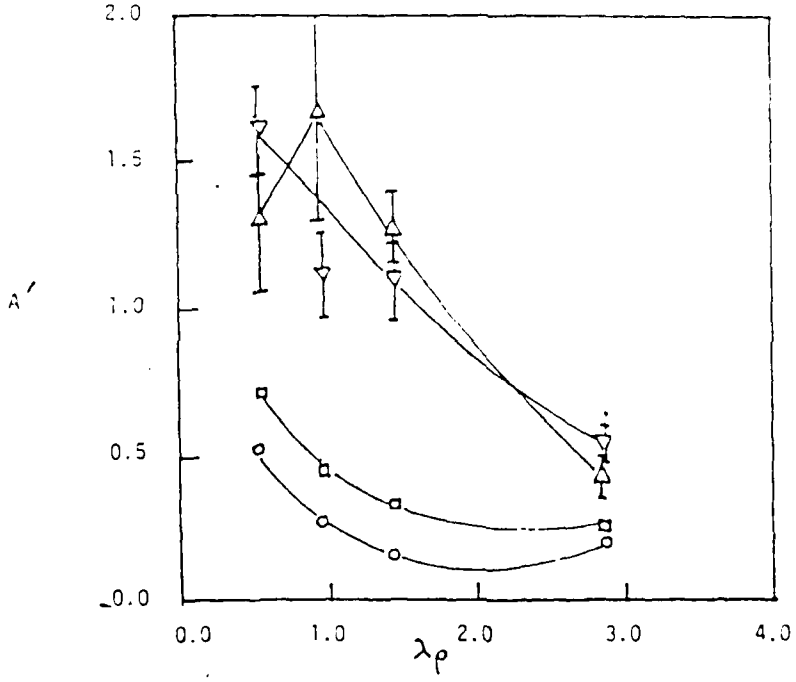

FIGURE 10 Parameter A' vs density ratio. Symbols are same as in Fig 10

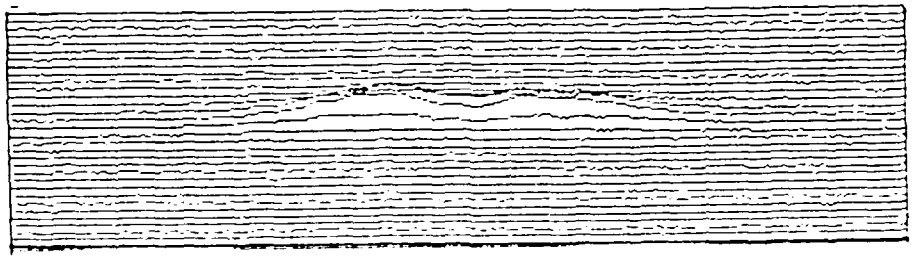

FIGURE 11 Intensity pattern for 86%He at M=0.6,1.0cm beam diameter,2.0cm down stream.

ICFM 1987

IN PROCEEDINGS of the INTERNATIONAL CONFERENCE ON FLUID MECHANICS
Beijing, CHINA

F-095

OPTICS OF INHOMOGENEOUS SHEAR LAYERS

W.H. Christiansen,* G. Yu,** D.W. Bogdanoff,+ T. Blum‡ and Y. Tsai‡
Aerospace and Energetics Research Program, University of Washington
Seattle, Washington 98195, U.S.A.

INTRODUCTION

Optical inhomogeneities in a flow field can seriously degrade the ability to focus a light beam through the flow field. There are many instances where one encounters turbulent interfaces in gas laser technology.[1] Shear layer and wakes occur in the resonators of high power lasers, for example. Coherent vortical structure may be present in the layer[2] and could cause large changes in refractive index as the layer entrains the ambient air. While some studies of laser beam degradation by shear layers have been carried out, they have for the most part ignored any ordered contribution and instead assumed spatially homogeneous turbulence.[3] Previous studies also used a narrow range of experimental parameters so that a study with a broader range of experimental conditions is warranted.

This paper is a continuation of previous work in the laboratory[4,5] in which the optical properties of a zero velocity ratio shear layer have been experimentally investigated. This involves a systematic investigation with independent control of density and compressibility effects. This was usually accomplished by using free jets of various helium and argon mixtures. Near-field information, such as spreading rate of shear layer, was mainly obtained from that of a large number of interferograms or schlieren photographs. Shear layer thickness measurements which cover a density ratio, λ_ρ, from 0.2 to 7.4 and Mach number, M, from 0.1 to 2.0 are presented.

While near field interferograms may be used to judge the source of beam distortion and magnitude and, in some instances, may be used

*Professor of Aeronautics and Astronautics.
**Visiting Scholar, Institute of Mechanics, Beijing.
+Research Engineer.
‡Graduate Student.

to calculate the far field effects, the measurement of the far field degradation is more accurate. This paper describes the technique that was used to obtain data directly from the far field of the laser beam after passing through the shear layer. The principal far field measurement used the Strehl ratio in which the time averaged peak intensity of a high quality He-Ne laser beam is measured in the far field with and without the shear layer present. The ratio of these two measurements is the Strehl ratio. This measurement was accomplished using digital optical imaging equipment whereby the far field data could be numerically processed by computer.

EXPERIMENTAL SETUP

Three contoured nozzles were employed for the investigation. They are 2-D symmetric nozzles with a square exit dimension of 1.4 cm. The ratio and angle of contraction at the entrance section were designed to minimize boundary layer growth. The contour in expansion section of the supersonic nozzles were designed to obtain uniform supersonic flow. The typical momentum thickness, θ at the nozzle exit, was calculated to be 0.027 mm for M = 0.1 and 0.058 mm for M = 1.4. The Reynolds number, based on the nozzle exit dimension and high speed gas stream, ranged from 3.1×10^4 to 75×10^4. The gases tested were He, Ar, CO_2, SF_6 and He-Ar mixtures of 95% He, 86% He, 62% He, 38% He and 27% He by volume. The flow was surrounded on three sides with optical glass which formed the test section (7.5 cm × 7.5 cm × 1.4 cm). A plane 2-D shear layer was formed at the fourth edge where the jet was allowed to mix with the ambient still air. An extension (7.5 × 32 × 1.4 cm) was placed downstream of the test section to eliminate anomalous entrainment of the ambient air in the test section.

For the near field investigations, conventional Mach-Zehnder (M-Z) interferometer, shear interferometer and schlieren were used to obtain information after passing through the shear layer. For the far field investigation, a diffraction-limited He-Ne laser beam was used to produce the Fraunhoffer diffraction pattern. The beam was spatially filtered, expanded, collimated, and then masked by a

circular aperture to produce a parallel test beam of nearly constant intensity. This beam was then passed through the mixing layer and then entered a reducing telescope to bring the diffraction-limited beam into a convenient range on the optical table. A (CCD type) electronic camera then captured the image of the diffraction pattern for digital storage and analysis on a computer.[6,7]

NEAR FIELD MEASUREMENTS

One of the length scales that characterize a shear layer is the thickness of the shear layer. The time averaged M-Z interferogram and shear interferograms of the shear layer were taken to obtain the mean growth rate of the index of refraction profiles. The process of data reduction may be found in Refs. 4 and 5. The M-Z interferometer was only functional at low Mach numbers due to vibration problems. However, the shear interferometer could still provide readable interferograms at Mach numbers up to 1.4.

The data was processed by a computer program that calculates self-similar profiles and the location of the virtual origin. The shear layer width is defined by the slope of straight line passing through relative index change of 0.1 and 0.9. The accuracy of the reading is believed to be around 0.2 fringe spacing. Figure 1 shows typical refractive index profiles plotted in nondimensional coordinates for the M-Z interferogram shown in Fig. 2. The various points refer to three axial locations and their near coincidence in nondimensional coordinates shows good self-similarity of the flow field.

Ensemble averaged schlieren photographs were also taken parallel to the shear layer. The visual growth rate of shear layer was measured by drawing straight line tangents to the edges of the shear layer, as done by Ref. 2. Considering the uncertainty in defining the edges of the layer, the error in growth rate is estimated to be 10-20%.

A set of complete data of both types of measurements is presented in Table 1. Correspondingly, the shear layer thickness, δ, vs. M and λ_ρ are presented in Figs. 3 and 4 respectively. The growth rates

decreased dramatically with increasing M and were only weakly dependent on λ_ρ. It can be seen from Fig. 4 that the growth rate varied more near the region of M=1 than elsewhere. The growth rate decreases 2.5-3.5 times as M goes from subsonic to supersonic. In contrast, the growth rate increases not more than 30% for an order and one-half increase in density ratio, as seen in Fig. 3. Coherent structure was only observed at $M < 0.6$ as determined by schlieren photographs.

Stop-action ruby laser interferograms taken normal to the shear layer gave near field results over the entire Mach number range. These pictures show that the He/air layer would produce the largest beam degradation, as can be seen in Fig. 5.

FAR FIELD MEASUREMENT

The optical data in this study are based on a reference beam formed by a plane wave incident on a circular aperture. The resulting far field diffraction pattern is the Airy pattern, which consists of a central bright spot known as the Airy disk surrounded by concentric subsidiary maxima.[8] The power in the beam within a radius r is found by integrating this far field intensity pattern over the area. The power vs. nondimensional radius is given in Ref. 8 and shows that 84% of the power is within the first ring of the ideal Airy pattern.

The Strehl ratio can be found by differentiating the power distribution with respect to r as r goes to zero. As the power is given by $p = 2\pi \int_0^r I_\zeta d\zeta$ for a symmetric pattern, then the intensity is given by

$$I = \lim_{r \to 0} \frac{d}{2\pi r dr} \left[\int_0^r 2\pi I_\zeta d\zeta \right] = \frac{1}{2\pi r} \frac{dp}{dr} . \qquad (1)$$

The Strehl ratio is thus found by taking the ratio of eq. (1) with and without flow. No tilt or focus correction was applied to these measurements.

Sutton[9] has derived a theoretical expression for the Strehl ratio assuming a homogeneous turbulence zone as

$$\frac{I}{I_0} = \exp[-\phi^2] = \exp[-2k^2 \langle \Delta n'^2 \rangle \Delta L] . \qquad (2)$$

$[-\phi^2]$ is the mean square phase error in the near field, Λ is the integral turbulence scale, L is the width of the zone, and $\langle \Delta n'^2 \rangle$ is the mean square refractive index perturbation in the zone. The results of the Strehl ratio study and shear layer growth study may be correlated. In a case where no coherent structure is seen, the scale length in the shear layer may be assumed to be 1/4 of to the measured shear layer thickness.[3] Under this condition, one may write

$$\frac{I}{I_o} = \exp[-k^2\alpha^2\Delta n^2\delta^2/2] \ , \qquad (3)$$

where Δn is the index refraction change across the layer and L is replaced by δ which is measured from the experiment. The constant, α, is then derived from the Strehl ratio. This permits a semi-empirical prediction of optical performance with respect to the mean thickness of the shear layer.

A time-averaged digitized electronic image of the laser beam was used as the principal measurement. Each image gives quantitative information on position and intensity of the laser beam in the far field. Experiments were run with various gases at different Mach numbers so beam degradation as a function of experimental parameters could be found.

Figures 6 and 7 show computer-drawn images of the far field with and without flow for 62% He mixture at M = 0.6. Each line in the figures represents the digitized signal from the corresponding line of the camera array. Only every sixteenth line is plotted and this is typical of the results found. The images in Figs. 6 and 7 are for an 0.5 cm beam and were taken with 0.1 sec exposure time. It was found that a decrease in beam diameter dramatically improved the Strehl ratio. For example, at M = 0.6 the Strehl ratio for 86% He ($\Delta n = 2\times10^{-4}$) decreases when beam diameter is increased from 0.5 cm to 1.0 cm at 1.0 cm downstream of the nozzle exit. Downstream location also has a large impact on Strehl ratio. An increase in downstream distance of 1.0 cm for 0.5 cm beam also decreases the Strehl ratio, as may be expected because of the increase in layer thickness. The variation of Strehl ratio with density ratios for M = 0.6, 0.9 and 1.4

were measured. As the spreading rate for all the shear layers increases with density ratio, increasing degradation with density ratio is expected.

Equation (4) relates the mean square phase error in the near field to Δn^2, δ^2, k^2 and a constant. The Strehl ratio data were plotted on a log scale versus $k\Delta n\delta$ for an 0.5 cm beam. A visual best fit straight line was drawn for each case. The lines fit the data well except CO_2. The slope of the line yields $\alpha^2/2$ which ideally should be constant. The values of α^2 were found to be quite variable but on the same order as those reported by others.[3] Attempts to fit the 1 cm beam data as above did not give a straight line, which leads one to believe the large beam is more affected by the inhomogeneous nature of the shear layer. The tabulated values of α and Strehl ratio for each measurement are given in Table II.

ACKNOWLEDGMENT

This work was supported by the air Force Office of Scientific Research. The imaging software was written by A. Westphal and D. Higgins and was invaluable to this work.

REFERENCES

[1] Christiansen, W.H., Russell, D.A., and Hertzberg, A., Ann. Rev. Fluid Mech. 7, 115 (1975).

[2] Brown, G.L. and Roshko, A., J. Fluid Mech. 64, 775 (1974).

[3] Vu, B.T., et al., AIAA paper No. 80-1414 (1980).

[4] Johari, H., et al., AIAA paper No. 84-1622 (1984).

[5] Christiansen, W.H., et al., "A Study of Inhomogeneous Shear Layers and Their Effect on Laser Beam Degradation," 5th GCL Symposium, Oxford, August 20-24, 1984.

[6] Higgins, D., "Laser Beam Degradation by an Inhomogeneous Free Jet Mixing Layer," Thesis, University of Washington, 1986.

[7] Thomas, T.C., "Far Field Optical Properties of Compressible Inhomogeneous Shear Layers," Thesis, Univ. of Washington, 1986.

[8] Principles of Optics, Born, M. and Wolf, E., 3rd ed., Pergamon Press, Oxford, 1964, pp. 395-398.

[9] Sutton, G., AIAA J 7, 1737 (1969).

TABLE 1

Gases & Mixtures	M	$\lambda_\rho = \frac{\rho_{air}}{\rho_{gas}}$	$\delta_{vis}/(x-x_0)$	$\delta/(x-x_0)$
SF_6	0.1	0.2	0.354	
CO_2	0.1	0.65	0.363	0.266
	0.6	0.58	0.300	0.197
	0.9	0.52	0.265	0.167
	1.4	0.40	0.105	
Ar	1.4	0.44	0.100	
	2.0	0.31	0.05	
27% He, 73% Ar	1.4	0.69	0.118	0.104
	2.0	0.41	0.077	
38% He, 62% Ar	0.1	1.10	0.365	0.27
	0.6	0.98	0.314	0.207
	0.9	0.87	0.281	0.184
	1.4	0.69		
62% He, 38% Ar	0.1	1.63	0.390	0.294
	0.6	1.46	0.340	0.22
	0.9	1.29	0.315	0.20
	1.4	0.99	0.171	0.15
86% He, 14% Ar	0.1	3.20	0.43	0.302
	0.6	2.96	0.373	0.25
	0.9	2.52	0.332	0.23
	1.4	1.93		
	2.0	[illegible]	0.178	
95% He, 5% Ar	0.1	4.39	[illegible]	0.321
	0.6	4.44	[illegible]	
	0.9	3.41	0.324	
	1.4	[illegible]	[illegible]	0.156
He	[illegible]	[illegible]	[illegible]	
	0.6	6.46	[illegible]	
	0.9	[illegible]	[illegible]	
	1.4	4.27	[illegible]	
	2.0	3.09	[illegible]	

Measured Shear Layer Thickness

TABLE 2

Diameter	I	M	λ_ρ	[illegible]	Strehl Ratio
0.5	1	0.1	0.65	0.12	0.8
0.5	1	0.1	1.1	0.107703	0.84
0.5	1	0.1	1.55	0.109627	0.6
0.5	1	0.1	2.2	0.092736	0.35
0.5	1	0.6	0.63	0.1	0.89
0.5	1	0.6	1	0.077459	0.98
0.5	1	0.6	1.45	0.070710	0.93
0.5	1	0.6	2.8	0.077459	0.77
0.5	1	0.9	0.55	0.118321	0.85
0.5	1	0.9	0.85	0.137638	0.92
0.5	1	0.9	1.3	0.223606	0.7
0.5	1	0.9	2.5	0.148323	0.56
0.5	1	1.4	0.4	0.148323	0.39
0.5	1	1.4	1	0.256324	0.93
0.5	1	1.4	3	0.2	0.78
0.5	2	0.1	0.65	0.12	0.45
0.5	2	0.1	1.1	0.091651	0.7
0.5	2	0.1	1.65	0.083442	0.39
0.5	2	0.1	2.2	0.067823	0.21
0.5	2	0.6	0.63	0.12	0.49
0.5	2	0.6	1	0.101980	0.88
0.5	2	0.6	1.45	[illegible]	[illegible]
0.5	2	0.6	2.8	0.08	0.4
0.5	2	0.9	0.55	[illegible]	[illegible]
0.5	2	0.9	0.85	[illegible]	[illegible]
0.5	2	0.9	1.3	[illegible]	[illegible]
0.5	2	0.9	2.5	[illegible]	[illegible]
1	1	[illegible]	[illegible]	[illegible]	[illegible]
1	[illegible]	[illegible]	[illegible]	[illegible]	[illegible]
1	[illegible]	[illegible]	[illegible]	[illegible]	[illegible]
1	[illegible]	[illegible]	[illegible]	[illegible]	[illegible]
1	[illegible]	[illegible]	[illegible]	[illegible]	[illegible]
1	[illegible]	0.6	1.45	[illegible]	[illegible]
1	1	0.6	2.8	[illegible]	[illegible]
1	1	1.4	[illegible]	[illegible]	[illegible]
1	[illegible]	1.4	1	[illegible]	[illegible]
1	1	1.4	3	[illegible]	[illegible]
1	2	[illegible]	0.55	[illegible]	[illegible]
1	2	[illegible]	[illegible]	[illegible]	[illegible]
1	2	0.6	[illegible]	[illegible]	[illegible]
1	2	0.6	1	[illegible]	[illegible]
1	2	[illegible]	1.45	[illegible]	[illegible]
1	2	[illegible]	2.8	[illegible]	[illegible]

Strehl Ratio Measurements & [illegible]

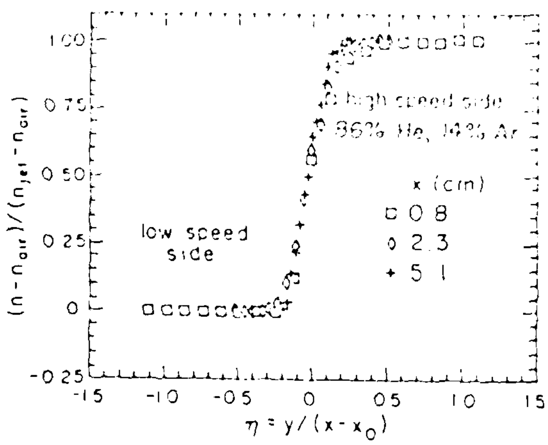

Fig. 1. Nondimensional Index Profiles for M=0.1 and λ_ρ = 3.2. x is the distance downstream of the nozzle exit.

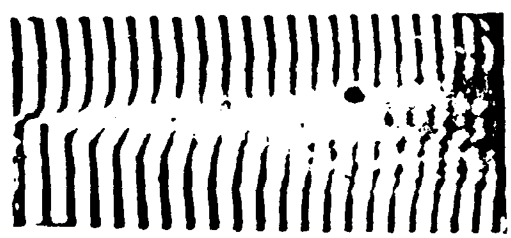

Fig. 2. Long Exposure Interferogram at M=0.1 and λ_ρ = 1.1. Gas jet is on top. Flow is from left to right.

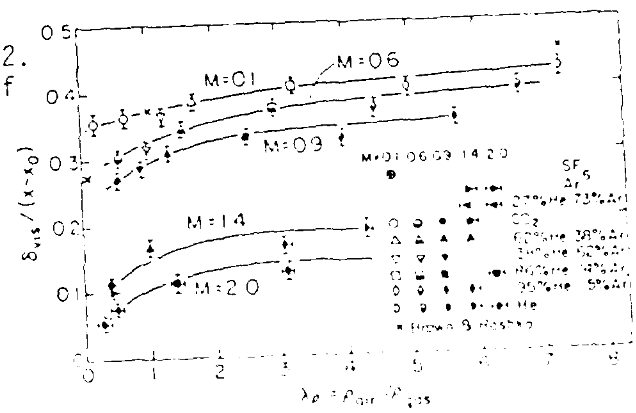

Fig. 3. Effect of λ_ρ on Spreading Rate. δ_{vis} = visual thickness of shear layer.

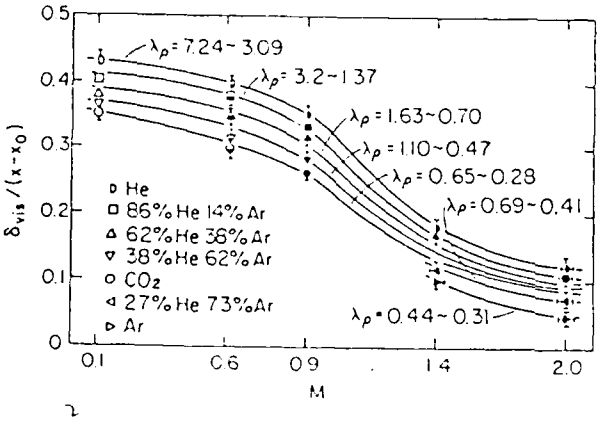

Fig. 4. Effect of M on Spreading Rate.

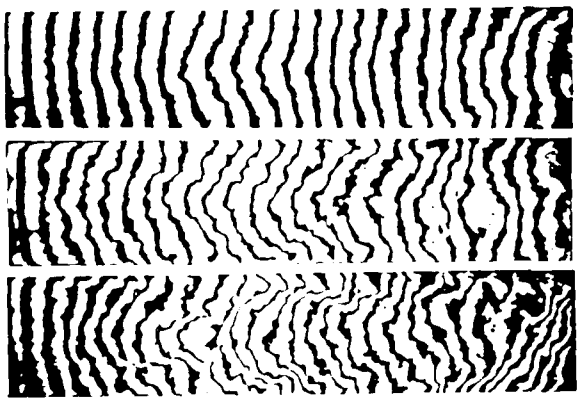

38% He 62% Ar
λ_ρ = 1.1

86% He 14% Ar
λ_ρ = 3.2

100% He
λ_ρ = 7.2

Fig. 5. Stop-Action Interferograms Normal to Shear Layer at M=0.1. Flow is from left to right.

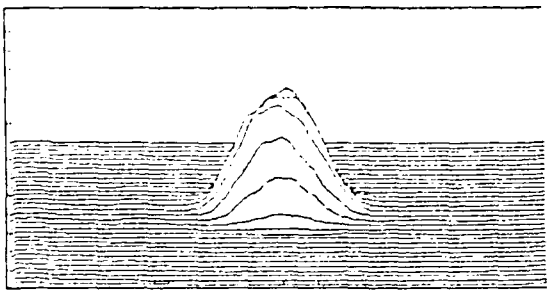

Fig. 6. Computer Drawn Image of a 0.5 cm Beam in the Far Field. Subsidiary maxima are lost in camera noise. Without flow.

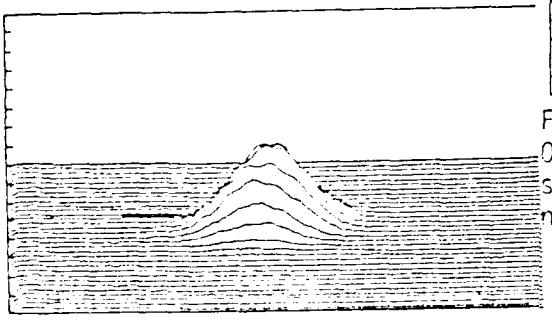

Fig. 7. Computer Drawn Image of a 0.5 cm Beam after Passing through a Shear Layer in the Far Field. x = 1.0 cm.

END

DATE

FILMED

MARCH

1988

DTIC